RESEARCH ARTICLE

REVISED Systems analysis of the prostate tumor suppressor NKX3.1 supports roles in DNA repair and luminal cell differentiation [version 2; referees: 2 approved]

Chih-Cheng Yang[1], Alicia Chung[5], Chia-Yu Ku[1], Laurence M. Brill[2], Roy Williams[3], Dieter A. Wolf[1,2,4]

[1]Tumor Initiation and Maintenance Program, Sanford-Burnham Medical Research Institute, La Jolla, CA 92037, USA
[2]NCI-designated Cancer Center Proteomics Facility, Sanford-Burnham Medical Research Institute, La Jolla, CA 92037, USA
[3]Informatics and Data Management Core, Sanford-Burnham Medical Research Institute, La Jolla, CA 92037, USA
[4]San Diego Center for Systems Biology, La Jolla, CA 92093-0375, USA
[5]Genentech Inc., South San Francisco, CA 94080, USA

v2 **First published:** 21 May 2014, **3**:115 (doi: 10.12688/f1000research.3818.1)
Latest published: 18 Dec 2014, **3**:115 (doi: 10.12688/f1000research.3818.2)

Abstract

NKX3.1 is a homeobox transcription factor whose function as a prostate tumor suppressor remains insufficiently understood because neither the transcriptional program governed by NKX3.1, nor its interacting proteins have been fully revealed. Using affinity purification and mass spectrometry, we have established an extensive NKX3.1 interactome which contains the DNA repair proteins Ku70, Ku80, and PARP, thus providing a molecular underpinning to previous reports implicating NKX3.1 in DNA repair. Transcriptomic profiling of NKX3.1-negative prostate epithelial cells acutely expressing NKX3.1 revealed a rapid and complex response that is a near mirror image of the gene expression signature of human prostatic intraepithelial neoplasia (PIN). Pathway and network analyses suggested that NKX3.1 actuates a cellular reprogramming toward luminal cell differentiation characterized by suppression of pro-oncogenic c-MYC and interferon-STAT signaling and activation of tumor suppressor pathways. Consistently, ectopic expression of NKX3.1 conferred a growth arrest depending on TNFα and JNK signaling. We propose that the tumor suppressor function of NKX3.1 entails a transcriptional program that maintains the differentiation state of secretory luminal cells and that disruption of NKX3.1 contributes to prostate tumorigenesis by permitting luminal cell de-differentiation potentially augmented by defects in DNA repair.

Open Peer Review

Referee Status: ✓ ✓

	Invited Referees 1	2
REVISED version 2 published 18 Dec 2014		
version 1 published 21 May 2014	✓ report	✓ report

1 **Kemal S. Korkmaz**, Ege University Turkey

2 **Philip D. Anderson**, Salisbury University USA

Discuss this article

Comments (0)

Corresponding authors: Chih-Cheng Yang (ccyang@sanfordburnham.org), Dieter A. Wolf (dwolf@sanfordburnham.org)

How to cite this article: Yang CC, Chung A, Ku CY *et al.* **Systems analysis of the prostate tumor suppressor NKX3.1 supports roles in DNA repair and luminal cell differentiation [version 2; referees: 2 approved]** *F1000Research* 2014, **3**:115 (doi: 10.12688/f1000research.3818.2)

Grant information: This work was supported by grant W81XWH-04-1-0167 from the Department of Defense Prostate Cancer Research Program to DAW. CCY is the recipient of a Prostate Cancer Training award from the Department of Defense Prostate Cancer Research Program (W81XWH-09-1-0423) and a trainee on the NCI-sponsored T32 Training Grant CA121949. The work was also supported by institutional grants P20 CA132386 and P50 GM085764. The generous support of Jeanne and Gary Herberger during the course of this work is gratefully acknowledged.
The funders had no role in study design, data collection and analysis, decision to publish, or preparation of the manuscript.

Competing interests: No competing interests were disclosed.

First published: 21 May 2014, **3**:115 (doi: 10.12688/f1000research.3818.1)

REVISED **Amendments from Version 1**

Version 2 contains the corrections requested by referee number 2; Philip D. Anderson

See referee reports

Introduction

NKX3.1 encodes a homeodomain transcription factor whose expression is largely restricted to the prostate and controlled by androgen. The gene is located on chromosome 8p21 in a region frequently deleted in early prostate cancers (reviewed in[1,2]). Studies in Nkx3.1 knockout mice have provided compelling evidence that Nkx3.1 is a prostate tumor suppressor[3–5]. These mice develop prostatic intraepithelial neoplasia (PIN), a precancerous lesion characterized by hyperproliferation of dysplastic cells, indicating that Nkx3.1 is haploinsufficient for PIN suppression[6]. Additional studies showed that serial passage of PIN-like lesions from Nkx3.1 mutant mice can undergo progressively severe histopathological alterations[5]. Finally, loss of Nkx3.1 can cooperate with loss of Pten and p27 in prostate cancer development in mice[7,8], while Nkx3.1 overexpression inhibits cell proliferation in Pten null epithelial grafts[9]. These data indicate that the diminished expression of NKX3.1 that is frequently observed in human prostate cancers[10] is involved in the initial stage of prostate carcinogenesis. While the tumor suppressor function of NKX3.1 remains poorly defined at the molecular level, the knockout phenotypes suggested that Nkx3.1 controls genes involved in prostate development, differentiation, and maintenance of tissue integrity.

Like other NKX class homeoproteins, NKX3.1 can function as a transcriptional repressor by binding a non-canonical homeodomain DNA motif such as naturally occurring in the mouse androgen receptor promoter[9] or artificially presented in synthetic reporter genes[11]. Transcriptional repression may involve NKX3.1-mediated recruitment of co-repressors[12] and the histone deacetylase, HDAC1[9]. A second mode of trans-repression found for the prostate-specific antigen (PSA) gene occurs independently of NKX3.1 promoter binding sites, but through repressive interaction with transcriptional activators such as SP1[13] and prostate-derived ETS factor (PDEF[14]). NKX3.1 was also shown to activate gene transcription, either through direct promoter binding as in the case of PCAN1 and HK2[15,16] or through interaction with other transcriptional activators such as serum response factor (SRF) or FoxA1 and the androgen receptor (AR)[17,18].

Transcriptomic profiling combined with global mapping of > 9,500 genomic binding sites by ChIP-sequencing revealed a set of 282 putative direct target genes that were differentially expressed in young NKX3.1$^{-/-}$ prostates not displaying PIN[16,19]. A subset of NKX3.1 target genes was also regulated by MYC with both transcription factors showing mutual antagonism[16]. Since overexpression of Myc cooperates with loss of Nkx3.1 in mouse prostate tumorigenesis, maintaining proper control of the common Nkx3.1/Myc target genes may be involved in Nkx3.1's tumor suppressor function[16]. A similar study in aged mice already displaying PIN revealed a gene expression signature indicative of impaired response to oxidative stress[20]. Interestingly, these changes correlated with a 5-fold increase in oxidative DNA damage in Nkx3.1$^{-/-}$ prostates. Whether oxidative DNA damage is a direct consequence of loss of NKX3.1 or a secondary consequence of PIN development is unknown.

Another key to understanding the tumor suppressor function of NKX3.1 potentially lies with its protein interaction partners. Several have been described that modulate NKX3.1's transcriptional effects (e.g. SRF[17,21], PDEF[14], HDAC1[9], SP1[13], MYC[16], and AR[18]). In addition, NKX3.1 was shown to bind to and augment the activity of topoisomerase I, suggesting that it functions in DNA repair[22,23]. NKX3.1 localizes to sites of DNA damage, promotes ATM and ATR activity, and enhances the survival of cells exposed to DNA damage[24]. Loss of NKX3.1 function in premalignant prostate cells may therefore accelerate the acquisition of DNA damage, potentially aggravated by unabated accumulation of reactive oxygen species thus promoting cellular transformation[24]. Nevertheless, it is currently unclear whether the function of NKX3.1 in DNA repair is indirectly mediated through transcriptional effects or directly through physical interactions with the DNA repair machinery.

In this report, we present an analysis of the NKX3.1 protein interactome that revealed intimate physical links of NKX3.1 with the DNA repair machinery, namely components of the DNA-dependent protein kinase (DNA-PK) holocomplex (XRCC5/Ku80, XRCC6/Ku70) and poly(ADP) ribose polymerase (PARP1). In addition, transcriptomic profiling of immortalized prostate epithelial cells upon acute activation of NKX3.1 revealed a rapid and complex transcriptional response that is a near mirror image of the gene expression signature of human PIN devoid of NKX3.1. Taken together, these data shed new light onto the elusive tumor suppressor activity of NKX3.1, directly implicating this homeoprotein in DNA repair and in driving a gene expression signature indicative of an essential function in maintaining the differentiation state of luminal prostate epithelial cells.

Materials and methods

Tissue culture, plasmids, viruses, antibodies

The human prostate cancer cell line LNCaP was obtained from ATCC and maintained in RPMI 1640 (Hyclone, Cat.# SH30027.01) supplemented with 10% fetal bovine serum (Sigma, Cat.# F6178-500ML), 50 units/ml penicillin, and 50 units/ml streptomycin (Thermo Scientific HyClone, Cat.# SV30010). The NKX3.1 cDNA was amplified from LNCaP mRNA, sequence confirmed, and cloned into pFLAG thereby attaching three consecutive FLAG epitope tags to the N-terminus. For DNA transfection, LNCaP cells were grown to 50–70% confluence on a 150 mm dish and transfected with 30 µg of plasmid DNA using DOTAP reagent according to the recommendations of the manufacturer (Roche, Indianapolis, IN). Immortalized human prostate epithelial cells (LH cells, kindly provided by Dr. W. Hahn;[25]) were maintained in Prostate Epithelial Cell Basal Media (Lonza, Cat.# CC-3165) including growth factors, cytokines, and supplements (PREGM Singlequots, Lonza, Cat. # CC-4177).

For production of adenoviruses, the ADEASY system was used as previously described[26]. The NKX3.1 cDNA was cloned into the pADTRACK1 shuttle vector. The resulting plasmid was transformed into BJ-ADEASY cells by electroporation. Adenoviral DNA generated by recombination in BJ-ADEASY cells was isolated and transfected into 293 cells (ATCC) using standard calcium

phosphate procedures. Virus was harvested from cells and amplified by infection of 293 cells. Amplified virus was tittered and used at a multiplicity of infection of ~100.

The following antibodies were used: Flag mouse monoclonal (Sigma-Aldrich Cat# F1804, RRID:AB_262044), NKX3.1 mouse monoclonal for immunoblotting (Invitrogen Cat# 35-9700, RRID:AB_138690), Anti-human NKX3.1 goat polyclonal (Santa Cruz Biotechnology, Inc. Cat# sc-15022, RRID:AB_650285) for immunoprecipitation, GFP mouse monoclonal (Clontech Cat# 632380, RRID:AB_10013427), actin mouse monoclonal (MP Biomedicals, Irvine, CA, Cat.# ICN691001), BANF rabbit polyclonal (EMD Millipore Cat# 09-893, RRID:AB_1977041), Ku70 mouse monoclonal (GeneTex Cat# GTX23114, RRID:AB_367103), Ku80 mouse monoclonal (GeneTex Cat# GTX72225, RRID:AB_383445), MYC rabbit polyclonal (Epitomics Cat# 1472-1, RRID:AB_562270), p21 rabbit monoclonal (Cell Signaling Technology Cat# 2947S, RRID:AB_823586), HSPA8 rabbit polyclonal (Sigma-Aldrich Cat# SAB2101098, RRID:AB_10604580), PARP mouse monoclonal (BD Biosciences Cat# 556494, RRID:AB_396433), HOXB13 rabbit polyclonal (Invitrogen Cat# 422500, RRID:AB_1500227).

FLAG-NKX3.1 affinity purification

Cells of one 150 mm dish transfected with pFLAF-NKX3.1 or empty vector were lysed in each 1 ml IP lysis buffer (50 mM Tris-HCl pH 7.4, 150 mM NaCl, 1% Triton X 100) on ice. Per affinity purification, 4 µg FLAG M2 antibody (Sigma-Aldrich Cat# F1804, RRID:AB_262044) was coupled to 50 µl magnetic beads in 0.2 M triethanolamine, pH 8.2 and 20 mM dimethyl pimelimidate with rotational mixing at room temperature for 30 min. The reaction was stopped by resuspending beads in 1 ml 50 mM Tris, pH 7.5 for 15 min. After five washes in IP lysis buffer, the beads were added to the cell lysate. Upon incubation for 4 h at 4°C, the lysate was removed and stored as "depleted lysates" at -20°C, whereas the beads were washed 5 times with 1 ml IP lysis buffer. After the final wash, beads were resuspended in 50 µl elution buffer (5 µg of triple FLAG peptide in PBS) and incubated at 4°C for 30 minutes with vortexing. The sample was analyzed by immunoblotting (10%), silver staining (2%), and LC-MS/MS (88%).

Liquid chromatography and tandem mass spectrometry (LC-MS/MS)

LC-MS/MS analysis of affinity purified FLAG-NKX3.1 complexes was performed as previously described in detail[27,28]. In brief, eluates were digested in solution with trypsin, and peptides were separated by reversed phase chromatography. Peptides were analyzed on an LTQ Orbitrap XL mass spectrometer (Thermo Fisher Scientific; San Jose, CA). The MS/MS method was top 4-data dependent. Dynamic exclusion was enabled. Data were searched against an international protein index (IPI) human protein database using Sorcerer-SEQUEST (SageN Research; Milpitas, CA).

Semi-quantitative analyses using spectral counting

Spectral counts are the number of times an ionized peptide isselected by the mass spectrometer for MS/MS, in the data-dependent mode and provide widely accepted, semi-quantitative estimates of relative protein abundance[29]. QTools, which are in-house developed visual basic macros (available from: www.dieter-wolf-lab.org/protocols) for automated spectral count analysis, were used to compute spectral counts of the proteins, using the PeptideProphet output from the trans-proteomic pipeline (TPP; Institute for Systems Biology, Seattle, WA;[30]).

Post-identification protein filtering

Purifications of FLAG-NKX3.1 were performed in quadruplicate (i.e. 4 biological replicates), each time starting with a fresh batch of cells. Altogether eight samples from affinity purifications (quadruplicates of mock and FLAG-NKX3.1) were analyzed repeatedly (3 times per sample, i.e. 3 technical replicates of each sample) by LC-MS/MS for a total of 24 LC-MS/MS runs.

Altogether we identified 315 human proteins (Data set 1A). To compile a high confidence NKX3.1 protein interactome, we first performed a background subtraction, i.e. the spectrum count obtained for each protein in the mock purifications was subtracted from the spectrum count obtained for that same protein in the corresponding FLAG-NKX3.1 purification (Data set 1B). The subtracted spectrum counts were then summed over all 4 independent purifications. If negative values were obtained after summing (i.e. if a protein was consistently more abundant in the mock purification than in the FLAG-NKX3.1 purification), the protein was disregarded. This resulted in a list of 250 proteins with an average spectrum count of 9.94 (Data set 1B). From this lists of background-subtracted data, we removed all proteins with spectrum counts below the average (≤ 10) to exclude low-abundance proteins potentially non-specifically associated with NKX3.1. This resulted in a list of 71 background subtracted and abundance-filtered proteins. In the next step, we collapsed redundant protein database entries (often resulting from multiple protein isoforms that were not distinguished by the peptides identified by LC-MS/MS) into single entries by adding their spectrum counts both in the mock and NKX3.1 purifications. This resulted in a non-redundant list of 58 proteins, which we refer to as the high confidence interactome (Data set 1B).

Since spectrum counts depend on protein size (larger proteins giving rise to more tryptic peptides), we normalized spectrum counts to protein molecular weights, which we have previously found to be an appropriate method of normalization[31]. The summed, normalized spectrum count numbers of all non redundant proteins were used to assemble the final background subtracted list of 58 NKX3.1 interacting proteins (referred to as Sum NKX3.1 – Mock). The summed normalized spectrum count numbers were also used to determine the fold enrichment of a protein in the NKX3.1 sample over mock (Sum NKX3.1/Mock). Both lists were sorted according to abundance and compared in Figure 1D to illustrate that both methods of background filtering (subtraction or division) yield an overlapping list of high confidence NKX3.1 interactors. The spectrum count intensity map in Figure 1C reiterates most of the steps described above thus presenting a comprehensive view of the analysis.

Reactome analysis

The NKX3.1 interactome was analyzed with the Cytoscape Reactome FI plugin[32]. The list of NKX3.1 interacting protein was loaded into Cytoscape and used to build Reactome networks allowing linker genes. The networks were clustered into modules, and pathways enriched in the modules (FDR ≤ 0.01) were identified (Figure 2A).

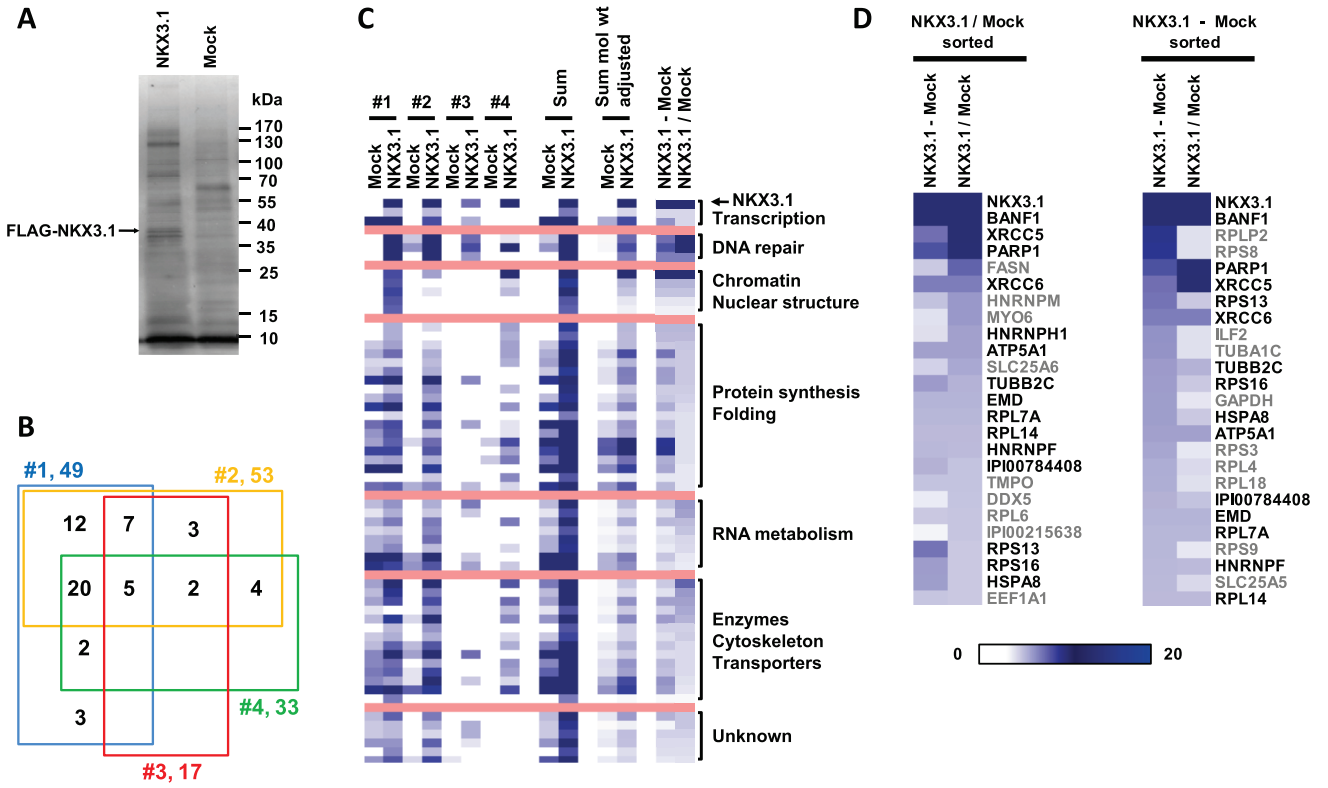

Figure 1. The NKX3.1 protein interactome. (**A**) Representative purification of FLAG-NKX3.1 from transfected LNCaP cells. Cell lysates were absorbed to anti-FLAG M2 resin, and specifically retained proteins were eluted with FLAG peptide and separated by SDS-PAGE. A band migrating with the expected molecular weight of FLAG-NKX3.1 and absent from the mock purification (empty vector) is highlighted. (**B**) Four-way Venn diagram to indicate the degree of overlap in the protein content detected in four independent purifications of FLAG-NKX3.1. (**C**) Map of spectrum count intensities in the four independent FLAG-NKX3.1 and mock purifications. The map also contains the sum of spectrum counts across all purifications as well as summed data after adjustment for protein molecular weights. The right most two columns present two distinct ways of background correction, either by subtracting mock values from NKX3.1 values (NKX3.1 – Mock) or by calculating the factor of enrichment in the NKX3.1 sample over mock (NKX3.1/Mock). See the Materials and methods section for details on data analysis and processing. (**D**) Spectrum count intensity maps of the 25 most abundant components of the NKX3.1 interactome. Data were sorted either by factor of enrichment (left panel, NKX3.1/Mock sorted) or by background subtracted values (right panel, NKX3.1 – Mock sorted). Black type font indicates the proteins occurring on both lists independent of the method of abundance-based sorting.

Transcriptome analysis

Duplicate RNA samples collected from NKX3.1 adenovirus transduced LH cells or from LH cells transduced with the GFP control virus were used for microarray analysis on the Illumina platform. The Human 6-V2 Expression BeadChips (Illumina) were used, which contain ~46,000 transcript probes. Primary data was collected using the manufacturer's BeadArray Reader using the supplied scanner software. Data analysis was done in three stages. First, expression intensities were calculated for each transcript probed on the array for all hybridizations using Illumina's Beadstudio#2 software. Secondly, intensity values were quality controlled and normalized. Quality control was carried out by using the Illumina Beadstudio detection p-value set to < 0.05 as a cutoff. This removed probes whose signals were too low to be reliably detected on the array. After this step, the initial ~46,000 probes were reduced to 22,319 (Data set 2A). Measurements were then normalized using the *normalize.quantiles* routine from the Affymetrix package[33] in Bioconductor (version 2.5, R version 2.10.1). This procedure accounted for any variation in hybridization intensity between the individual arrays. An assessment of several different normalization techniques using the Bioconductor *maCorrPlot* routine suggested that *normalize.quantiles* was the most appropriate for the data. Finally, these normalized data were imported into GeneSpring and analyzed for differentially expressed genes. The raw datasets were submitted to the GEO database (accession number GSE47030).

To identify genes differentially expressed between LH cells infected with Ad-GFP and Ad-GFP-NKX3.1 the biological replicates for each time point (7 h and 10 h) were averaged. Datasets were interrogated for genes with statistically significant differences between the two groups (i.e. +/- NKX3.1) based on the results of the Welch t-test (parametric test, variances not assumed equal; p-value cutoff 0.05). To find the genes with the most robust changes in expression, the data was plotted as a "Volcano Plot" (Supplementary Figure S2B), which allows statistical significance to be measured along with the

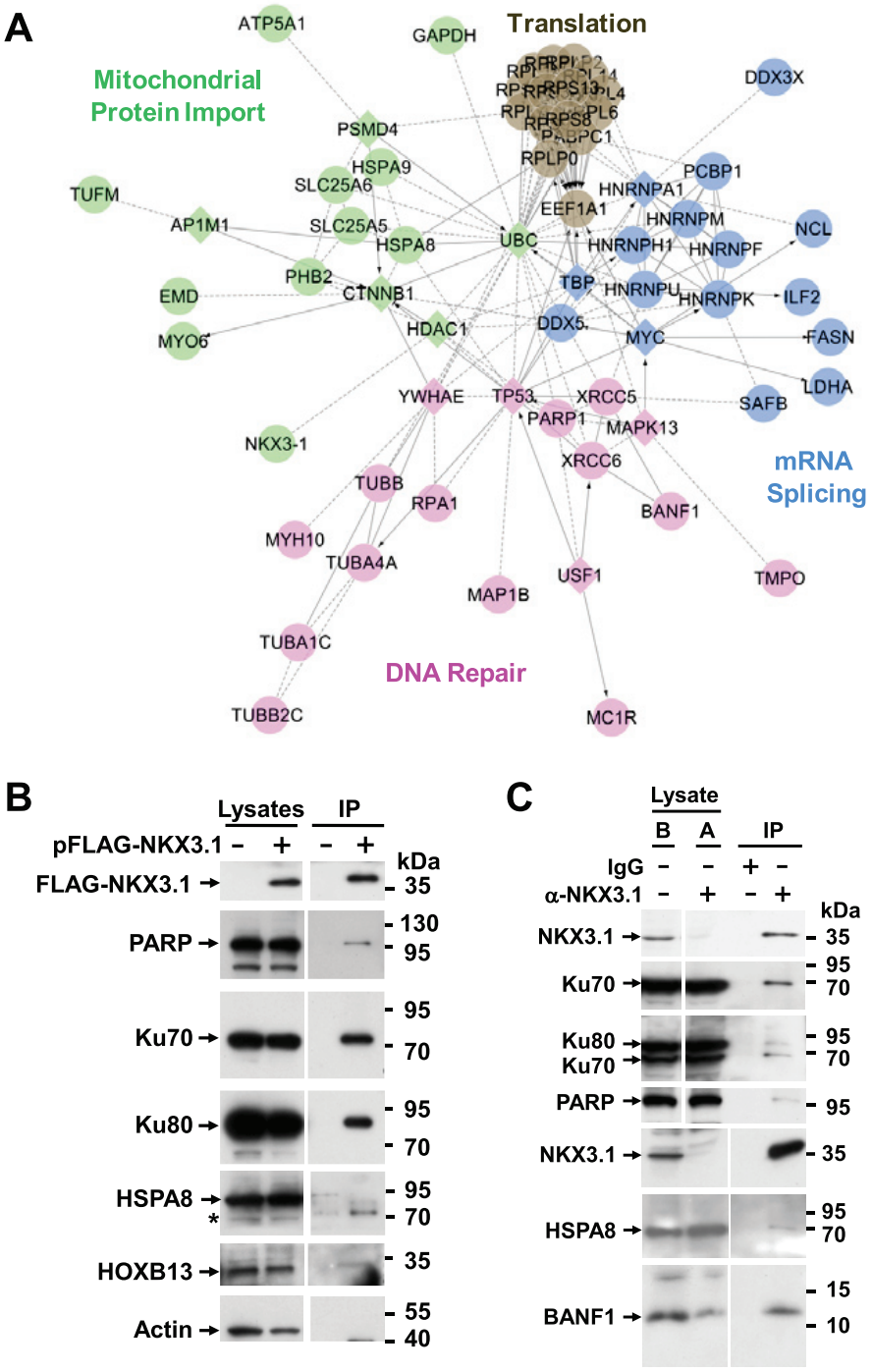

Figure 2. NKX3.1 interacts with DNA repair proteins. (**A**) The list of NKX3.1 interacting proteins was loaded into Cytoscape and used to build Reactome Functional Interaction networks. The networks were clustered into modules (indicated by colors), and pathways enriched in the modules (FDR ≤ 0.01) were identified. Diamonds represent network components that were not identified as NKX3.1 interacting proteins. (**B**) LNCaP cells were transfected with FLAG-NKX3.1 (+) or empty vector (-) followed by absorption of cell lysate to FLAG M2 resin to purify FLAG-NKX3.1. Co-purifying DNA repair proteins were detected by immunoblotting. The bottom four panels are from the same affinity purification resolved on a separate gel. The asterisk denotes an unspecific cross-reactivity of the HSPA8 antibody. Cropped blot images are shown; see Figure S7 for full images. (**C**) A nuclear protein fraction was prepared from LNCaP cells and employed for immunoprecipitation with NKX3.1 antibodies or an IgG control as indicated. The same samples before ("B") and after ("A") immunoprecipitation are shown to document the specific depletion of endogenous NKX3.1. The bottom three panels are from the same immunoprecipitate resolved on a separate gel. Cropped blot images are shown; see Supplement Figure S7 for full images.

extent of fold change in expression. Lists of mRNAs significantly changing 3-fold or 5-fold upon expression of NKX3.1 were assembled (Data set 2C).

RNA isolation and Q-PCR analysis

LH cells were infected with 20 µl of Ad-GFP or Ad-GFP-NKX3.1 viruses and total RNA was isolated after 6, 8, 10, and 12 h using the RNeasy mini kit (Qiagen, Valencia, CA). RNA concentrations were determined by measuring absorption at 260 nm in a spectrophotometer. Aliquots of 2 µg of total RNA from each sample were reverse-transcribed into cDNA using an Omniscript RT kit (Qiagen) according to the manufacturer's instructions. Quantitative Real-Time PCR was performed using Brilliant SYBR Green QPCR Master Mix (Stratagene, La Jolla, CA) and the Mx3000 Real-Time PCR System (Stratagene). Gene specific primers were designed using the Primer3 algorithm (http://frodo.wi.mit.edu/) as shown below. PCR reactions were run according to the protocol for the Brilliant SYBR Green QPCR Master Mix. Briefly, PCR was carried out using a final concentration of 0.2 µmol of the primer pairs, 50 ng of cDNA template and 12.5 µl of Brilliant® SYBR Green QPCR Master Mix. The volume was adjusted to 25 µl by adding RNase-free water. The thermocycling protocol began with a 3 min denaturation at 95°C, a 40 cycle amplification program consisting of 30 s denaturation at 95°C, 1 min annealing at 55°C and 30 s extension at 95°C. Upon conversion of raw ct values to linearly related X(0) values, expression values were normalized to GAPDH, and expression changes were expressed as ratios of mRNA levels in NKX3.1 infected versus GFP infected cells (NKX3.1/GFP). The ratios were log2 transformed and averaged across two technical replicates, and standard deviations were calculated.

Primer sequences used for Q-PCR:

HSPA6_F	CCGTGAAGCACGCAGTGAT
HSPA6_R	ACGAGCCGGTTGTCGAAGT
TAGLN_F	GCTGGAGGAGCGACTAGTGG
TAGLN_R	CCTCCTGCAGTTGGCTG
CDH2_F	TGGAACGCAGTGTACAGAATCAG
CDH2_R	TTGACTGAGGCGGGTGCTGAATT
CCND2_F	TACCTTCCGCAGTGCTCCTA
CCND2_R	TCACAGACCTCCAGCATCCA
STAT2_F	CACCAGCTTTACTCGCACAG
STAT2_R	TGGAAGAATAGCATGGTAGCCT
EEF1A2_F	GCTGAAGGAGAAGATTGACC
EEF1A2_R	TTCTCCACGTTCTTGATGAC
CDKN1A_F	TTGTCTTTCCTGGCACTAAC
CDKN1A_R	CCCTCGAGAGGTTTACAGTC
HES1_F	GCATCTGAGCACAGAAAGTC
HES1_R	CTGTCATTTCCAGAATGTCC
S100A2_F	GGGAAATGAAGGAACTTCTG
S100A2_R	CACATGACAGTGATGAGTGC
TNFa_F1	GTGGACCTTAGGCCTTCCTC
TNFa_R1	ATACCCCGGTCTCCCAAATA
TNFa_F2	CCCAGGCAGTCAGATCATCTT
TNFa_R2	TCTCAGCTCCACGCCATT

Measurement of cell proliferation

LH cells were seeded in 384-well plates at a density of 2000 cells per well. After 24 hours, cells were transduced with Ad-GFP-NKX3.1 or control Ad-GFP adenoviruses for the times indicated in Figure 6D–F. Proliferation (i.e. DNA synthesis) was measured using the Click-iT® EdU Alexa Fluor® 594 HCS kit (Invitrogen, Carlsbad, CA) according to the manufacturer's instructions. Briefly, 10 µM 5-ethynyl-2′-deoxyuridine (EdU) was added to culture media for one hour, and cells were fixed with 3.7% formaldehyde, washed with PBS twice, permeabilized with 0.1% Triton X-100 in PBS, stained with Click-iT Alexa Fluor 594 dye, and counterstained with 1 µg/mL Hoechst 33342 (Blue). Plates were scanned and analyzed by using a Celigo automated cytometer at dual wave length to detect Hoechst dye (total cell count) and Alexa Fluor 594 (cells incorporating EdU and thus undergoing DNA synthesis). Four images per well were obtained at each wave length, and the percentage of proliferating cells was calculated by dividing the number of Alexa positive cells by the total cell number.

MAP kinase inhibitors and neutralizing antibodies were added two hours after viral transduction. JNK inhibitors SP600125 (EMD Chemicals Inc, San Diego, CA) and p38 inhibitor SB203580 (Enzo Life Sciences, Farmingdale, NY) were used at 20 µM. Mouse IgG directed against TNFα (Clone *6401,* R&D Systems, Minneapolis, MN) and whole mouse IgG as a control (Jackson ImmunoResearch Laboratories, West Grove, PA) were used at 5 µg/ml.

Pathway and network analysis

Ingenuity Pathway Analysis (IPA, Ingenuity Systems) was used for pathway and network analysis. The bulk of the analysis was performed with the 5× dataset (mRNAs showing a significant ≥ 5-fold change upon expression of NKX3.1). The 3× dataset was used for the MYC network. Datasets were imported into IPA, and analyzed with the following settings: Reference Set: Ingenuity Knowledge Base (Genes + Endogenous Chemicals); Network Analysis: Direct and Indirect Relationships; Data Source: Ingenuity Expert Findings; Confidence: Experimentally Observed; Species: Mammal (human, mouse, rat) and Uncategorized (e.g. chemicals); Tissue and Cell Lines: All.

NextBio analysis

The 5× dataset was uploaded to the NextBio server through the Sanford-Burnham portal. 153 of the 158 features of the 5× dataset were recognized and could be interpreted by NextBio. The analysis was performed using default settings. Significantly enriched transcription factor binding sites were identified through corresponding Biogroups. The overlap between the 5× dataset and the gene expression study by Nanni *et al.*[34] was identified through a search against all curated studies.

Indirect immunofluorescence staining

Flag-NKX3.1 transfected LNCaP cells were seeded onto 15 mm poly-lysine coated glass cover slips, and fixed using formaldehyde (3.7% in PBS). Samples were stained with mouse monoclonal FLAG (Sigma) or goat polyclonal NKX3.1 antibodies (Santa Cruz). Alexa Fluor 568 (red) donkey anti-mouse IgG and Alexa Fluor 488 (green) donkey anti-goat IgG conjugate antibodies (Life Technologies Cat# A10037, RRID:AB_11180865 and Cat# A11055, RRID:

AB_10564074) were used as secondary antibodies. The nuclei were stained with 4'–6' diamidino-2-phenylindole (DAPI). Samples were imaged on a Nikon Type 120 inverted fluorescent microscope using 60× magnification.

Results

The NKX3.1 interactome

Reasoning that the NKX3.1 interactome may be most effectively profiled in cells that naturally express this protein, we transiently expressed FLAG epitope-tagged NKX3.1 in LNCaP human prostate cancer cells. FLAG-NKX3.1 was approximately 5-fold in excess over endogenous NKX3.1 (Supplementary Figure S1A) but localized primarily to cell nuclei (Supplementary Figure S1B). The proteasome inhibitor MG132 was added 4 hours prior to lysate preparation in order to slow the rapid clearance via the ubiquitin-proteasome pathway to which NKX3.1 is normally subjected[35,36]. Cell lysate was absorbed to anti-FLAG M2 resin, and specifically retained proteins were eluted with FLAG peptide. Four independent affinity purifications were performed in parallel with mock purifications of lysate of cells transfected with empty vector. The eluates were examined by SDS-PAGE (Figure 1A) and subjected to LC-MS/MS analysis in order to determine their protein composition. Altogether, 315 proteins were identified at a false-positive rate of ≤ 0.01 (Data set 1A).

The protein dataset was subjected to background subtraction and abundance-based filtering to arrive at a list of 58 high confidence NKX3.1 interacting proteins (see Materials and methods and Data set 1B). Fifty five of the 58 proteins were identified in at least two independent purifications, and 27 were identified in at least three purifications (Figure 1B, Data set 1C). Five proteins were consistently identified as NKX3.1 interaction partners in all four independent purifications, namely NKX3.1, the DNA repair proteins XRCC5/Ku80 and PARP1, and the protein synthesis proteins RPS9 and PABPC1.

We next performed a relative quantification of the NKX3.1 interactome based on spectral counting[29]. Upon summing the molecular weight adjusted spectrum counts of each protein across the four mock and NKX3.1 purifications, we derived background corrected quantifications by either subtracting summed mock values from summed NKX3.1 bait values (NKX3.1 – Mock) or by dividing NKX3.1 bait values from mock values (NKX3.1/Mock) to obtain the factor by which a protein was enriched in the NKX3.1 bait samples over the mock sample. Both methods confirmed the expectation that NKX3.1 was the most abundant protein identified in the FLAG affinity purifications (Figure 1C, D). We also performed Reactome Functional Interaction analysis to construct a functional interaction network of NKX3.1 binding proteins derived from manually curated literature data[32]. The network was clustered into modules and enriched functional pathways/reactions were identified (Figure 2A).

Among the 10 most abundant co-purifying proteins were the components of the DNA-dependent protein kinase (DNA-PK) holoenzyme, XRCC5/Ku80, XRCC6/Ku70, and poly(ADP) ribose polymerase (PARP1) (Figure 2A). DNA-PK and PARP1 have important functions in DNA double strand break repair, recombination, and telomere maintenance but are also involved in chromatin and transcriptional control[37–39]. For example, Ku proteins associate with a series of homeodomain proteins (HOXC4, OCT1, OCT2, DLX2) thereby recruiting them to DNA ends where they are phosphorylated by DNA-PK[40]. Such phosphorylation was proposed to lead to DNA damage-dependent changes in their transcriptional activities. ADP-ribosylation mediated by PARP1 can stimulate the ability of DNA-PK to phosphorylate protein substrates[41]. Our interactome data provide a possible mechanism underlying the previously observed localization of NKX3.1 to sites of DNA damage[24], although the functional consequences of these interactions for NKX3.1 transcriptional activity remain to be established. Regardless, follow-up co-immunoprecipitation experiments showed that overexpressed NKX3.1 readily interacted with endogenous XRCC5/Ku80, XRCC6/Ku70, and PARP1 (Figure 2B). Interaction of DNA-PK with ectopically expressed NKX3.1 was very recently reported in an independent study[42]. We show here that endogenous NKX3.1 also interacts with XRCC5/Ku80, XRCC6/Ku70, and PARP1 (Figure 2C).

Among the top ranking NKX3.1 interacting proteins was also interleukin enhancer binding factor 2 (ILF2/NFAT 45 kDa) (Figure 1D). This protein was previously shown to interact with the DNA-PK-Ku complex[43] and to be part of a ribonucleoprotein assembly containing heterogeneous nuclear ribonucleoproteins (hnRNPs), the heat shock protein HSPA8, the poly-A binding protein PABC1, nucleolin (NCL), and several ribosomal proteins[44], all of which were also identified here as components of the NKX3.1 interactome (Figure 1C, D, Data set 1A). Most of these interactions were also represented in the Reactome network (Figure 2A). Two additional subunits of this particle, ILF3 and YBX1 were also identified, albeit at low levels (Data set 1A). hnRNPs function in multiple processes, including mRNA splicing, dynamics, stability, and translation, telomere maintenance, DNA repair, and chromatin remodeling and transcription[45]. They are also major constituents of the nucleolar proteome, which additionally comprises many of the NKX3.1 interacting proteins listed above, including the DNA-PK complex, PARP1, HSPA8, and ribosomal proteins as well as the RNA helicases DDX3 and DDX5[46,47]. Although the significance of these interactions remains unclear, they may reflect a close physical coupling of NKX3.1-dependent mRNA transcription to mRNA processing[48] and/or hitherto unappreciated role for NKX3.1 in nucleolar ribosome biogenesis and cytoplasmic mRNA transport. A similar proposition was made to rationalize the interactome of the transcription factor SOX2, which shares remarkable overlap with the NKX3.1 interactome[49].

Another highly abundant NKX3.1 interactor is the chromatin and nuclear assembly regulator BANF1 (Figure 1D). This interaction was confirmed by co-immunoprecipitation (Figure 2B). BANF1 was previously shown to bind two other proteins identified in the NKX3.1 interactome, emerin (EMD) and thymopoetin (TMPO)[50]. In addition, BANF1 interacts with several other homeodomain transcription factors and regulates the transcriptional activity of one of them, CRX[51]. It is thus likely that BANF1, in complex with emerin and thymopoetin, is involved in NKX3.1-mediated gene regulation. The nuclear matrix attachment proteins SAFA/HNRNPU and SAFB, which were also identified as NKX3.1 interacting proteins, may also participate in this process.

Finally, we identified an interaction of NKX3.1 with the homeobox transcription factor HOXB13 (Data set 1C). This interaction was confirmed by co-immunoprecipitation (Figure 2A). HOXB13 also interacts with the androgen receptor and regulates the cellular response to androgen[52]. In addition, germline mutations of HOXB13 significantly increase risk of hereditary prostate cancer through unknown mechanisms[53]. However, further studies discounted the intriguing possibility that mutation of HOXB13 alters its interaction with NKX3.1 (CCY & DAW, unpublished observation).

NKX3.1-induced transcriptional program

Previous determinations of NKX3.1-dependent gene expression signatures have profiled prostates of mice that developed and aged in the complete absence of NKX3.1[16,19,20]. These signatures may therefore describe adaptive changes that occur in response to long-term depletion of NKX3.1 in addition to its immediate effects on gene expression. We have therefore chosen to acutely introduce NKX3.1 into immortalized human prostate epithelial cells (LH cells[25]) that do not express detectable levels of NKX3.1 protein (data not shown). We produced adenoviruses driving the expression of either GFP alone or GFP and NKX3.1 from separate promoters (Ad-GFP and Ad-GFP-NKX3.1 viruses, respectively). LH cells were infected with these viruses according to the scheme in Figure 3A. GFP signal became first detectable by live cell fluorescence microscopy 6 hours after infection (data not shown). We therefore harvested duplicate cultures of cells for immunoblotting 7 and 10 hours after infection and determined that NKX3.1 and GFP were expressed at both time points (Figure 3B). No cytopathic effects of adenovirus infection were observed within the time frame of the experiment. In parallel, we prepared duplicate RNA samples of the 7 hours and 10 hours time points for transcriptome analysis.

The global changes in transcript levels noted in response to NKX3.1 expression were very similar at the 7 hours or 10 hours time points (Supplementary Figure S2A). Statistically significant changes were observed for several hundred mRNAs. To reduce the

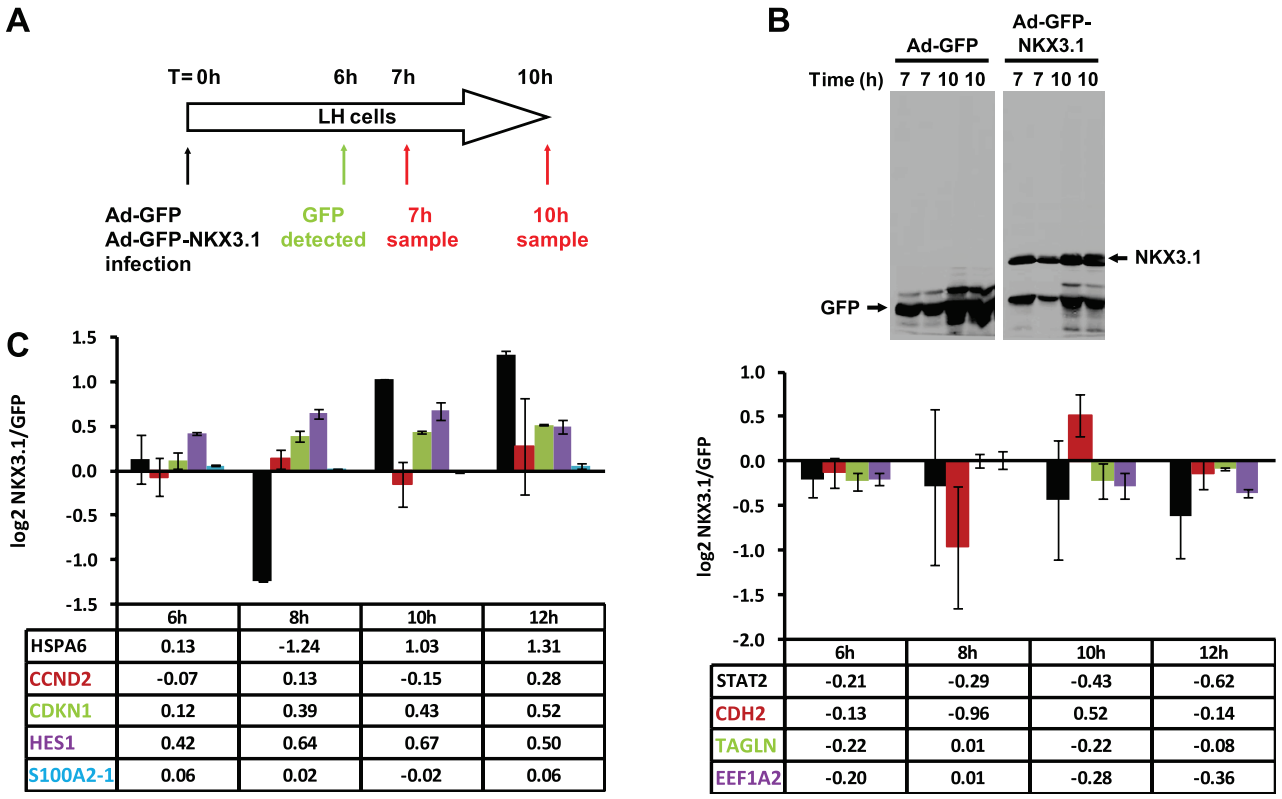

Figure 3. Adenovirus-mediated expression of NKX3.1 in LH prostate epithelial cells regulates specific mRNAs. (**A**) Schematic representation of the time course of the experiment. LH cells were infected in duplicate with adenoviruses driving the expression of either GFP alone or GFP and NKX3.1 from two separate promoters. GFP expression became first apparent by fluorescence microscopy 6 hours after transfection (data not shown). (**B**) Duplicate cell lysates were prepared 7 and 10 hours after infection, and examined for the expression of GFP and NKX3.1 by immunoblotting. NKX3.1 expression was already detectable at the earliest time point (7 hours). (**C**) Quantitative RT-PCR analysis of 9 mRNAs whose expression is changed in response to NKX3.1. LH cells were infected with adenoviruses driving the expression of either GFP alone or GFP and NKX3.1, and mRNA was isolated after the indicated time points (6, 8, 10, 12 hours). The RNA samples were analyzed by Q-PCR, and expression values are shown as log2 transformed ratios of the mRNA level in NKX3.1 infected versus GFP infected cells (NKX3.1/GFP). Error bars indicate standard deviations obtained from two replicate measurements. The left panel shows data for 5 mRNAs that were upregulated by NKX3.1 in the array dataset, whereas the right panel shows data for four mRNAs that were downregulated.

number of mRNA changes to be further interrogated to a manageable number, we arbitrarily set a cut-off of 5-fold change. This yielded lists of 158 differentially expressed genes for the 7 hours time point (Supplementary Figure S2B) and 165 for the 10 hours time point. Since there was a considerable overlap of both lists, we limited the further analysis to the 7 hours sample. Data sets 2A and B summarize all mRNA expression data. Supplementary Table 1 presents a ranked list of all 107 mRNAs with > 5-fold upregulation, whereas Supplementary Table 2 presents a corresponding list of all 51 mRNAs with > 5-fold downregulation in NKX3.1 expressing LH cells (see also Data set 2C). We chose 5 upregulated and 5 downregulated mRNAs for validation by Q-PCR with a fresh set of replicate RNA samples prepared from cells infected with Ad-GFP or Ad-GFP-NKX3.1 for increasing periods of time. Nine out of the 10 expression changes confirmed the tendency seen from microarrays, although variability was substantial for some measurements (Figure 3C). We failed to confirm the induction of KRT17 mRNA apparent from the array data (not shown). Additional validation by Q-PCR and immunoblotting is shown in various sections below (see Figure 6).

Examination of the lists of mRNA changes revealed a fundamental reprogramming of gene expression in LH cells upon acute expression of NKX3.1. Overall, the changes were indicative of inhibition of cell proliferation and induction of cell differentiation. For example, 9 epithelial differentiation markers (cytokeratins 5, 6B, 7, 8, 17, 18, 19, stratifin, kallikrein 5) were strongly induced. In addition, the Notch pathway, which is often downregulated in prostate cancers[54], was induced (DLL1, HES1, JAG2). The cyclin-dependent kinase inhibitor p21 (CDKN1A), which inhibits cell cycle progression and induces cell differentiation[55], was also increased.

Reassuringly, many of the strongest NKX3.1-induced mRNAs encode proteins that were previously shown to be downregulated in human prostate cancer based on immunohistochemistry (Supplementary Table 1). This included, for example, the calcium binding proteins S100A2 and A14[56], the 14-3-3 protein stratifin[57,58], laminin A[59], claudin 7[60], prostasin[61], P cadherin[62], and kallikrein 5[63]. Cyclin D2 is considered an activator of cell cycle progression but was induced by NKX3.1. Remarkably, however, cyclin D2 is typically downregulated in human prostate cancers[64]. Four mRNAs encoding HSP70s were upregulated (Supplementary Table 1). HSP70 expression is frequently lost in aggressive prostate cancers[65] and experimental HSP70 overexpression inhibits the tumorigenicity of prostate cancer xenografts in mice[66]. Likewise, three genes encoding the HSP70 co-chaperones DnaJ/HSP40 were upregulated > 5-fold. Lastly, two glutathione transferases were upregulated by NKX3.1, a finding that is consistent with the previous demonstration that NKX3.1 upregulates oxidative stress defense[20].

The list of downregulated genes (Supplementary Table 2) included genes involved in cell migration (actin/myosin-related, collagens 1A1, 5A1, 5A2), several growth factors, and the interferon/STAT pathway. Many of the most downregulated genes were previously shown to be overexpressed in prostate and other cancers (Supplementary Table 2). This applies, for example, to eukaryotic translation elongation factor 1 alpha (EEF1A2) which is a potential oncogene[67], the BMP antagonist gremlin 1[68], and the transcription factor FOXD1[69]. N-cadherin, which is frequently found to replace epithelial cadherin forms in prostate cancers ("cadherin switch") was also strongly downregulated[70]. Significantly, NKX3.1 also upregulated P cadherin thus reversing the cadherin switch.

We also compared our list of 357 mRNAs that were changed ≥ 3-fold by NKX3.1 with a recent list of 282 mouse genes thought to be direct NKX3.1 targets based on a combination of expression and ChIP-seq data[16]. Despite the species difference and the diametrical strategies (overexpression versus knockout), 10 genes were represented on both lists (Supplementary Table 3). This overlap is highly significant when considering that 8 out of these 10 genes were regulated by NKX3.1 in the same direction.

Pathway analysis

To assess functional modules and signaling pathways affected by NKX3.1, we performed a global analysis with the Ingenuity Pathway Analysis (IPA) package. The analysis was performed with the dataset of mRNAs changing more than 5-fold ("5× dataset") or, where indicated, with a larger dataset of mRNAs changing more than 3-fold ("3× dataset", 357 genes). Since identical top scoring pathways were obtained with both datasets, the analysis was largely restricted to the smaller 5× dataset, unless otherwise noted.

Consistent with the involvement of NKX3.1 in prostate development, we found highly significant overrepresentation of IPA "Functions" pertaining to development, cell movement, proliferation and cell growth (Figure 4A). Of particular interest was the term "Reproductive Systems Disease", which included the subgroup "Prostatic intraepithelial neoplasia" (PIN). PIN is the earliest known precursor lesion of prostate cancer, and frequently shows decreased NKX3.1 levels[71]. The "PIN" Function contained the seven genes listed in Figure 4B. A previous study determined that six of these genes were downregulated in PIN versus normal prostate, whereas one was upregulated[72]. Remarkably, five out of the seven genes displayed a mirror image of the changes occurring in PIN when examined in NKX3.1-expressing LH cells (Figure 4B). These findings suggest that changes in gene expression in early PIN may be causally linked to loss of NKX3.1.

As shown in Figure 4C, a number of pathways were overrepresented that were not readily apparent from the manual curation of the gene lists presented above. For example, the analysis indicated upregulation by NKX3.1 of the p53 and IL1 pathways, in addition to the Notch signaling pathway. Interferon signaling, in turn, appeared to be switched off by acute NKX3.1 expression.

Network analysis

TNFα network. To obtain a better understanding of the regulatory circuitry underlying NKX3.1-induced modulation of particular functional pathways, we performed network analysis using Ingenuity IPA software. The highest ranking network presented in Figure 5A featured TNFα, a gene that was induced by NKX3.1 (Supplementary Table 1, Figure 6A), in the center with edges reaching to 27 distinct nodes. Eighteen of these edges were defined by a gene regulatory relationship (i.e. expression edge) thus signifying genes that are known to be either induced or suppressed by TNFα

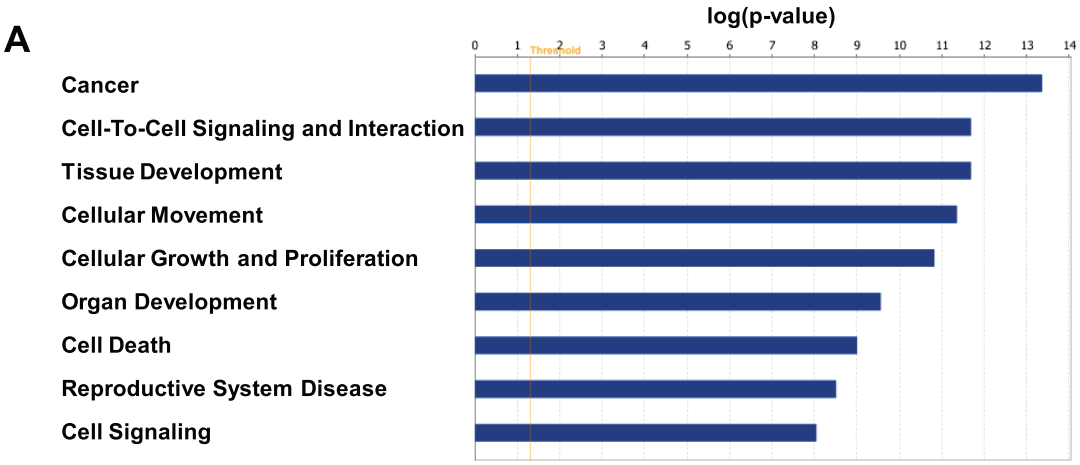

B

Genes with inverse expression in PIN and LH-NKX3.1 cells

Gene	PIN	LH -NKX3.1	Description
C3	↓	↑	Complement component 3, peptidase
CDH3	↓	↑	P cadherin
ITGB4	↓	↑	Integrin beta 4
KRT7	↓	↑	Keratin 7
MYL9	↓	↓	Myosin light chain 9
SIM2	↑	↓	Single-minded homolog 2, transcription factor
VCAN	↓	↓	Versican, cell adhesion

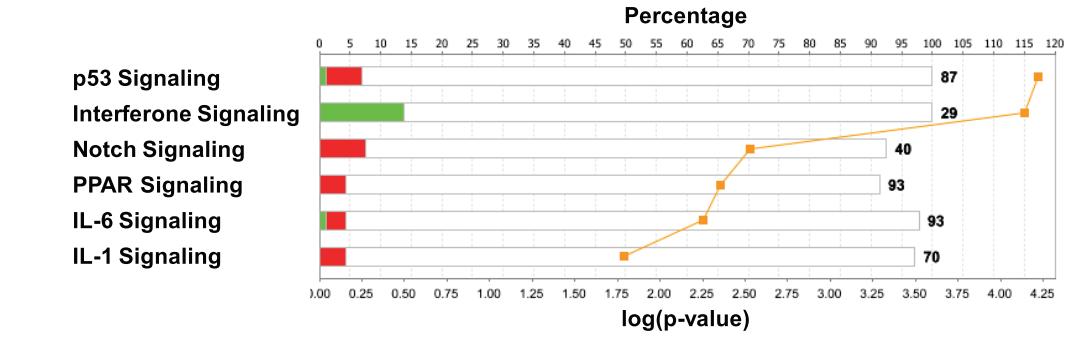

Figure 4. Functions and pathways that are overrepresented in the NKX3.1 gene expression program. (**A**) Select IPA "Functions" significantly overrepresented in the 5× mRNA set. (**B**) List of mRNAs with inverse expression in prostatic intraepithelial neoplasia (PIN;[72]) and NKX3.1 expressing LH cells. mRNAs shown in red are upregulated whereas those shown in green are downregulated. (**C**) Select IPA "Canonical Pathways" overrepresented in the 5× dataset. The abscissa on the top indicates the percent fraction of all possible pathway components that were represented in the dataset. Since this dataset only contained a relatively small number of 158 mRNAs, a small percent wise overrepresentation of pathway components is statistically highly significant ($p < 0.05$, see yellow graph).

signaling. Further annotation of the TNFα network also connected TNFα to NKX3.1-induced suppression of cell movement through downregulation of action-myosin based mobility components and enhancement of cell adhesion through upregulation of laminins (Figure 5A). Both processes are considered bona fide hallmarks of tumor suppression. Close examination of every TNFα expression edge revealed considerable concordance between the definition of the edge (based on the published literature) and the actual expression of the target node in response to NKX3.1. Fourteen first degree nodes predicted to be activated by TNFα were also upregulated by NKX3.1 (Supplementary Table 4). Consistent with MAP kinase signaling being a major downstream pathway activated by TNFα, we found that a chemical inhibitor of JNK but not p38 could partially antagonize NKX3.1-induced expression of HSPA6 and HES1 (Figure 6B).

p53 network. Another high scoring network featured the tumor suppressor p53 at the center with first degree edges to 8 nodes.

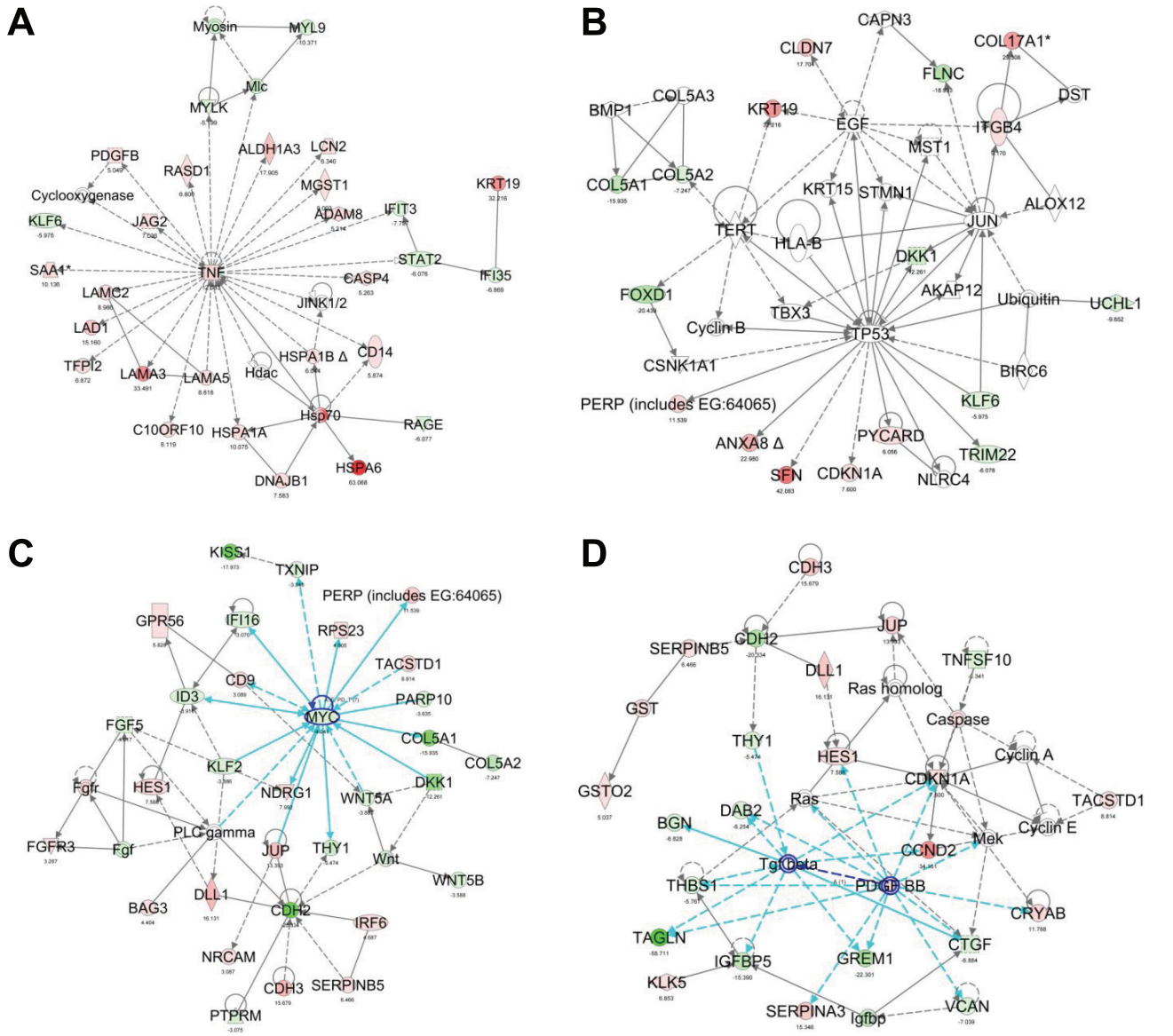

Figure 5. IPA network analysis of the NKX3.1 transcriptional program. (**A**) TNFα network. Node colors represent the level of up- (red) or down- (green) regulation upon expression of NKX3.1. (**B**) Tumor suppressor p53 network. The p53-TERT-EGF-JUN quadrangle is highlighted by dark blue edges. (**C**) MYC network. First degree edges of MYC are highlighted in light blue. (**D**) PDGFB/TGFβ network. First degree edges are highlighted in light blue, the PDFGB-TGFβ link in dark blue.

Although p53 was upregulated neither at the mRNA nor protein level (Figure 6C), a finding which is consistent with the well-established activation of p53 at the post-translational level, the network indicated robust induction of some of its known target genes. As shown in Figure 5B, this included the 14-3-3 sigma protein stratifin (SFN), an epithelial differentiation marker missing from many prostate cancers[57,73], the cyclin-dependent kinase inhibitor p21 (CDKN1A,[74]), and the p53 apoptosis effecter PERP[75]. Induction of p21 protein by NKX3.1 was confirmed by immunoblotting (Figure 6C). Annexin A8 (ANXA8) is also known to be upregulated by p53[76]. Using the 3× dataset, we pinpointed an additional 7 mRNAs that are upregulated by NKX3.1 as known targets of p53 (Supplementary Figure S3). These findings suggested that the p53 tumor suppressor pathway is activated by acute induction of NKX3.1 in LH cells. The network contained three additional highly connected nodes, telomerase (TERT), EGF, and JUN, which formed a quadrangle with p53. Although JUN mRNA was not induced by NKX3.1, a positive effect of p53 on JUN was reported previously[77].

MYC network. A further high scoring network that was obtained with the 3× dataset was organized around the MYC oncogene (Figure 5C). MYC itself was 4-fold downregulated by NKX3.1 expression, an effect that was validated by immunoblotting

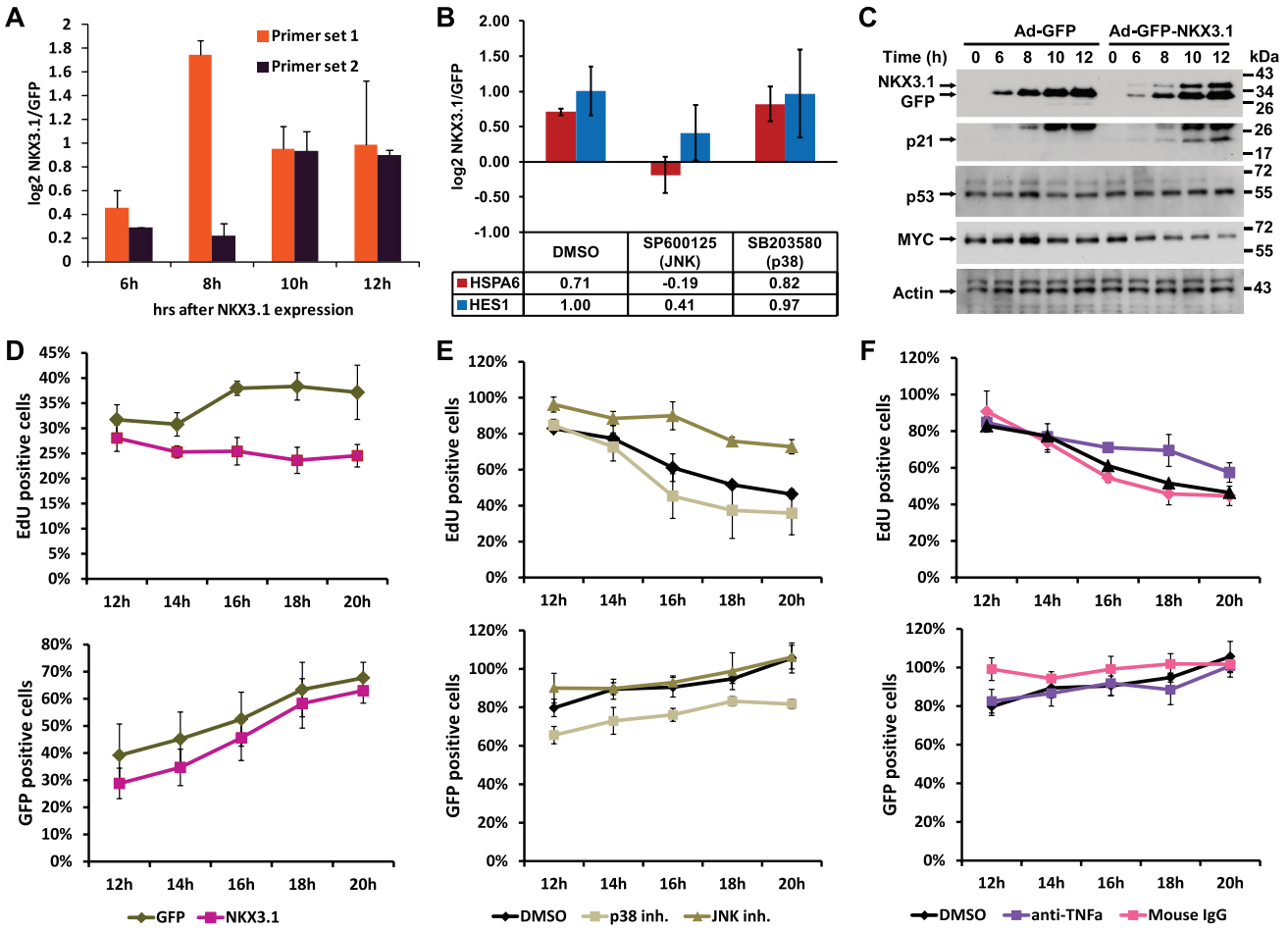

Figure 6. NKX3.1-induced changes in gene and protein expression. (**A**) Quantitative RT-PCR analysis of TNFα mRNA. LH cells were infected with adenoviruses driving the expression of either GFP alone or GFP and NKX3.1, and mRNA was isolated after the indicated time points (6, 8, 10, 12 hours). The RNA samples were analyzed by Q-PCR with two different primer sets amplifying TNFα mRNA, and expression values are shown as log2 transformed ratios of the mRNA level in NKX3.1 infected versus GFP infected cells (NKX3.1/GFP). Error bars indicate standard deviations obtained from two replicate measurements. (**B**) LH cells were infected with adenoviruses driving the expression of either GFP alone or GFP and NKX3.1. After 4 hours, 10 μM of the JNK inhibitor SP600125 or 10 μM of the p38 kinase inhibitor SB203580 were added followed by mRNA isolation after 6 hours. The levels of HSPA6 and HES1 were analyzed by Q-PCR. Expression values are shown as log2 transformed ratios of the mRNA level in NKX3.1 infected versus GFP infected cells (NKX3.1/GFP). Error bars indicate standard deviations obtained from two replicate measurements. (**C**) LH cells were infected with adenoviruses driving the expression of either GFP alone or GFP and NKX3.1, and protein lysates were prepared after the indicated time points (6, 8, 10, 12 hours). The expression of the indicated proteins was determined by immunoblotting. Cropped blot images are shown; see Figure S8. for full images. (**D**) LH cells were infected with Ad-GFP and Ad-GFP-NKX3.1 viruses, and the rate of DNA synthesis was measured by EdU incorporation after the indicated times (top graphs). The percentage of GFP positive cells was determined as a measure of infection efficiency (bottom graphs). (**E**) LH cells were infected with Ad-GFP-NKX3.1 virus, and the effect of JNK inhibitor (SP600125, 20 μM) or p38 kinase inhibitor (SB203580, 20 μM) on NKX3.1-mediated suppression of DNA synthesis was measured by EdU incorporation. The percentage of GFP positive cells was determined as a measure of infection efficiency (bottom graphs). (**F**) LH cells were infected with Ad-GFP-NKX3.1 virus, and the effect of neutralizing antibodies to TNFα or control IgG on NKX3.1-mediated suppression of DNA synthesis was measured by EdU incorporation. The percentage of GFP positive cells was determined as a measure of infection efficiency (bottom graphs).

(Figure 6C). This coincided with downregulation of several genes that were previously found to require MYC function for their expression (TXNIP, IFI16[78]). In addition, the MYC interaction partner PARP10 was downregulated upon expression of NKX3.1. Conversely, two genes that are negatively regulated by MYC were activated upon NKX3.1 expression (PERP[79], NDRG[80]), suggesting that NKX3.1-induced downregulation of MYC relieves its repressive effect on these genes. In aggregate, these findings suggest that restoration of NKX3.1 expression in LH cells led to downregulation of pathways normally turned on by MYC. This may contribute to a block in proliferation and promote cell differentiation by NKX3.1. Antagonism of NKX3.1 and MYC in target gene regulation and prostate tumorigenesis was recently also demonstrated in a mouse model[16].

PDGFB/TGFβ network. Another network featured PDGFβ (PDGFB and PDFGBB), which was induced 5.1-fold by NKX3.1. The induction of PDGFB mRNA and the expression of many of its first degree interacting nodes, is consistent with PDGFB signaling being upregulated by NKX3.1. For example, three nodes that were upregulated by NKX3.1 (CRYAB, SERPINA3, CDKN1A) and two nodes that were downregulated (DAB2, TAGLN) were previously shown to be controlled by PDGFB in the same manner (Supplementary Figure S4;[81,82]). PDGFB is also known to activate PPAR/RXRα-dependent transcription. Notably, RXRα is itself upregulated by NKX3.1 (5.7-fold), hence explaining the overrepresentation of PPAR signaling in the canonical pathway analysis above (Figure 4C). Since PPAR signaling is known to suppress prostate cancer cell proliferation[83], it may be relevant to NKX3.1-mediated tumor suppression.

PDGFB shares a number of nodes with another growth factor, TGFβ (Figure 5D). Although TGFβ1 mRNA was not altered by NKX3.1, the more abundantly expressed TGFβ2 was downregulated (Supplementary Table 5). Most first-degree nodes emanating from TGFβ were downregulated by NKX3.1 expression (Supplementary Figure 3). An additional 25 genes in the TGFβ signaling pathway were either downregulated or unchanged by NKX3.1, further suggesting that NKX3.1 does not activate TGFβ signaling (Supplementary Table 5). Since TGFβ is a strong driver of the epithelial-to-mesenchymal transition (EMT,[84]), NKX3.1-mediated suppression of TGFβ signaling may contribute to its differentiation-inducing activity.

Network connectivity

In an attempt to obtain a more cohesive view of the global effects of NKX3.1 on prostate gene expression, we merged individual networks. For simplicity, only expression edges were included in Figure 7A. Not only were TNFα and p53 directly linked through an expression-based edge, but several of their individual first degree nodes were targets of edges emanating from both TNFα and p53. For example, TFP12 and CASP4 are positively regulated by both TNFα and by p53[77,85–87].

The AP1 transcription factor subunit JUN, which was part of the p53 network (Figure 5B) was linked to TNFα resulting in a triangular configuration (Figure 7A). Whereas both TNFα and p53 are known to stimulate the expression of JUN and AP1 activity[77,88], NKX3.1 expression did not significantly affect the mRNA level of cJUN (-1.21-fold change) or JUND (+1.25-fold change). However, the JUN interaction partner FOS was increased 3.9-fold by NKX3.1. Since FOS maintains exactly the same edges within the network as JUN (data not shown), AP1 transcriptional activity appears to be upregulated in response to NKX3.1 expression.

Finally, we manually integrated the TNFα network with the connections to all major factors the network analysis had implicated in the NKX3.1 transcriptional program, including FOS/AP1, MYC, and p53. Despite the complexity of the resulting network, a tentative framework for NKX3.1-induced transcriptomic changes is becoming readily apparent (Figure 7B, C). According to this framework, NKX3.1 expression in LH cells results in the activation of the TNFα pathway. This in turn leads to activation of the p53, Notch, PDGFB, and AP1 pathways. Conversely, the MYC and interferon/STAT pathways are turned off. Through Q-PCR and immunoblotting, we have already confirmed several of these predictions (see Figure 3C for p53, Notch, PDGFB, STAT, and Figure 6 for TNFα, MYC, and p53). In addition, transduction with NKX3.1 expressing virus led to growth inhibition of LH cells relative to virus

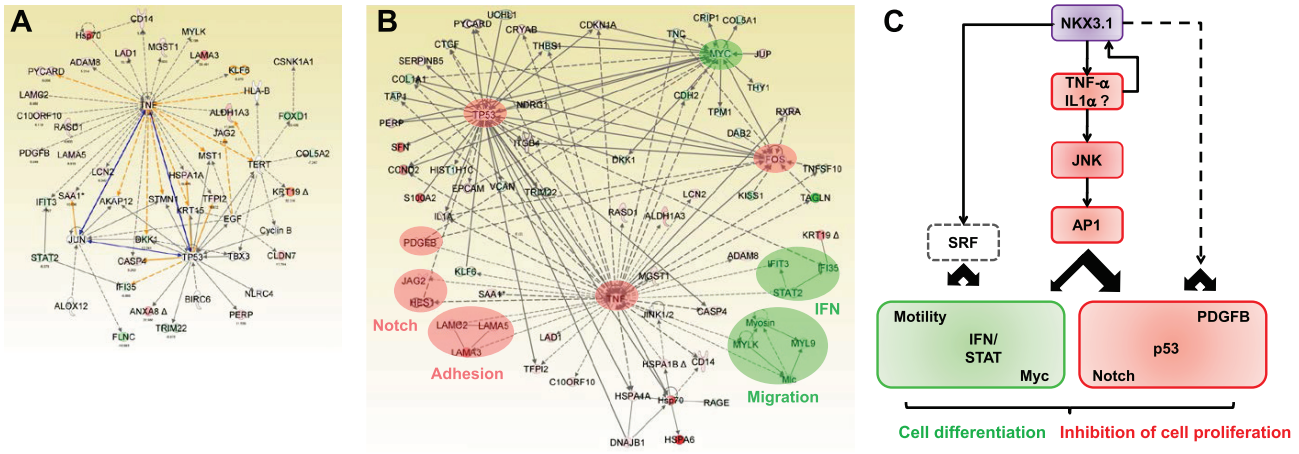

Figure 7. Framework of the NKX3.1 transcriptional program. (**A**) The merged TNFα-p53 network. Network links are highlighted in yellow. Direct edges between TNFα, p53, and JUN are emphasized in blue color. (**B**) Construction of a network containing the major factors implicated in the NKX3.1 transcriptional program, including FOS/AP1, MYC, and p53. Modules activated by NKX3.1 expression are shaded in red and those suppressed in green. (**C**) Tentative framework of NKX3.1-dependent changes to cellular modules. Based on the induction of TNFα and FOS mRNA by NKX3.1, and the antagonistic effects of JNK inhibitors on NKX3.1-mediated gene expression and cell proliferation, the framework proposes that TNFα signaling results in activation of AP1 and modulation of downstream genes and functional modules (red squares symbolize upregulation/activation, green squares downregulation). Additional pathways (stippled lines) may impinge on SRF and other transcription factors (not shown).

expressing GFP alone (Figure 6D). Notably, growth inhibition was partially rescued by JNK inhibitor and by a neutralizing antibody against TNFα (Figure 6E, F). These observations further support a role of NKX3.1 in inducing a block to cell division and promoting cell differentiation via a TNFα/JNK/AP1-dependent pathways.

Enrichment of transcription factor binding sites

We next employed the NextBio platform to relate our expression data to previously published large-scale genomics data. One dataset that matched with high statistical significance (p = 4.5E-11) featured a set of 1082 genes containing evolutionarily conserved genomic binding sites for AP1[89]. Twenty six of these genes were represented in our list of ~150 NKX3.1 responsive genes with 20 being induced by NKX3.1 (Supplementary Table 1, Supplementary Table 2, Supplementary Figure 5A, Data set 2D). Combined with the evidence from network analysis and the upregulation of FOS, these findings suggest that NKX3.1 causes AP1 activation and/or cooperates with AP1 in gene activation. Consistent with this conjecture is the well-known induction of JUN N-terminal kinase (JNK) activity by TNFα signaling, which enhances the transcriptional activity of JUN. Finally, NFκB which is also induced by TNFα signaling, can cooperate with AP1 at some promoters[90].

A second DNA binding motif that was overrepresented ($p = 1.6E^{-5}$) in NKX3.1 responsive genes conforms to a binding site for serum response factor (SRF). 216 human genes contain the serum response element (SRE) motif in a promoter proximal context that is conserved in mouse, rat, and dog[89]. These 216 genes included 9 genes that were represented on our dataset, all but one of which was suppressed by NKX3.1 (Supplementary Table 2, Supplementary Figure 5B, Data set 2E). Since NKX3.1 is known to physically interact with SRF[17], our data strongly suggests that NKX3.1 cooperates with SRF in transcriptional suppression.

Comparison with human prostate cancer data

Nextbio analysis also revealed a highly significant match with a study comparing gene expression in human prostate cancer tissues[34]. This study profiled 22 cell lines derived from surgical samples of prostate cancer patients with clinically localized disease and absence of hormonal neo-adjuvant treatment before surgery. In keeping with these selection criteria for early cancers, the cell lines (and primary tumors they were derived from) had suffered loss of 8p21 (i.e. NKX3.1) but did not display genetic abnormalities typical of more advanced prostate cancers (e.g. loss of PTEN, amplification of MYC and androgen receptor). 3415 mRNAs were significantly changed in prostate cancer cell lines relative to normal prostate.

Of 153 differentially expressed genes in our dataset, 82 (53%) were also changed in prostate cancer derived cell lines (PCaDCL), a highly significant overlap ($p = 2.0E^{-36}$, Supplementary Figure 6; Data set 2F). Of the 82 overlapping genes, 60 were downregulated and 22 were upregulated in PCaDCL versus PrEC. Strikingly, 93% of the mRNAs downregulated in PCaDCL were induced by expression of NKX3.1 in LH cells (Supplementary Table 1). In addition, 19 of the 20 genes upregulated in PCaDCL were downregulated by NKX3.1 (Supplementary Table 2). Moreover, many of the mRNA expression changes observed in the PCaDCL microarray study were independently confirmed at the protein level by immunohistochemistry of prostate cancer tissue samples (Supplementary Table 1 and Supplementary Table 2). These analyses strongly suggest that the principal gene regulatory networks that are affected by NKX3.1 expression in LH cells are inversely perturbed in early human prostate cancer marked by loss of this tumor suppressor.

NKX3.1 expression and interactions Dataset

9 Data Files

http://dx.doi.org/10.6084/m9.figshare.1002064

Discussion

We have employed a series of global approaches to explore the tumor suppressor function of NKX3.1. The NKX3.1 interactome revealed a complex pattern of interactions with DNA repair proteins and with other transcriptional regulators such as ILF2 and BANF1 that predict a similarly complex transcriptional program enacted by NKX3.1. Indeed, global analysis of the gene expression pattern actuated by acute expression of NKX3.1 in immortalized human prostate epithelial cells with a basal phenotype (LH cells[25,91]) revealed a rapid and extensive re-programming with 158 mRNAs changing ≥ 5-fold and 331 mRNAs changing ≥ 3-fold. This complex pattern was interrogated by network analysis to account for the recognition that representation of cellular processes and reactions as linear pathways is often an oversimplification that does not accurately reflect the complexity of intracellular wiring[92].

Network analysis indicated NKX3.1-dependent modulation of a series of interconnected functional modules and enabled a tentative framework for the transcriptional program induced by NKX3.1 in human prostate epithelial cells. Broadly speaking, NKX3.1 activation culminates in the downregulation of cellular motility as well as MYC and IFN/STAT activity and in the upregulation of p53 activity, the Notch pathway, and PDGF signaling (Figure 7C). Many of these changes are readily consistent with the tumor suppressor function of NKX3.1 observed in knockout mice[3–5].

Importantly, network analysis allowed us to pinpoint several unanticipated pathways on which NKX3.1 appears to impinge. For example, the analysis suggested a major role for TNFα whose mRNA was induced by NKX3.1. TNFα is a well-established inducer of MAP kinase signaling, including JNK and p38 kinases. Significantly, IL1α was also induced by NKX3.1 (Supplementary Table 1) hus further augmenting MAPK activation. JNK activates AP1 transcriptional activity thus readily rationalizing the strong over representation of AP1 binding sites in NKX3.1 responsive genes. Localized NKX3.1-mediated TNFα-JNK signaling in prostate epithelial cells may promote and maintain their differentiation state thus suppressing tumorigenesis. The important role of JNK signaling in cell differentiation is well established[93,94]. The finding that pro-inflammatory cytokines also destabilize NKX3.1 protein[36] indicates a negative feedback loop that may counteract their pro-apoptotic function (Figure 7C).

Importantly, the NKX3.1-induced gene signature is, to a large extent, a mirror image of the gene expression pattern found in early human

prostate cancers devoid of NKX3.1[34]. This inverse pattern further suggests that NKX3.1 is a key driver of luminal cell differentiation, whereas loss of NKX3.1 would allow luminal cells to dedifferentiate into a state with higher proliferative capacity thus making them more vulnerable to the acquisition of additional oncogenic events perhaps augmented by concurrent defects in DNA repair. Clearly such additional events are essential for prostate carcinogenesis given that PIN in NKX3.1 knockout mice does not progresses to overt prostate cancer, unless further genetic changes are incurred[5–8].

Data availability

figshare: NKX3.1 expression and interactions Dataset. Doi: 10.6084/m9.figshare.1002064[95]

Author contributions

CCY performed the NKX3.1 affinity purifications and the biochemical experiments confirming protein interactions. He also performed validation of microarray data by Q-PCR and immunoblotting. AC prepared NKX3.1 adenoviruses and performed the microarray experiment. CYK assisted with tissue culture and the affinity purifications. LMB performed mass spectrometry of NKX3.1 interacting proteins. RW performed statistical analysis of microarray data and assisted in pathway analysis. DAW conceived the study, performed pathway and network analysis using IPA, and drafted the manuscript.

Competing interests

No competing interests were disclosed.

Grant information

This work was supported by grant W81XWH-04-1-0167 from the Department of Defense Prostate Cancer Research Program to DAW. CCY is the recipient of a Prostate Cancer Training award from the Department of Defense Prostate Cancer Research Program (W81XWH-09-1-0423) and a trainee on the NCI-sponsored T32 Training Grant CA121949. The work was also supported by institutional grants P20 CA132386 and P50 GM085764. The generous support of Jeanne and Gary Herberger during the course of this work is gratefully acknowledged.

The funders had no role in study design, data collection and analysis, decision to publish, or preparation of the manuscript.

Acknowledgements

We are grateful to Dr. W. Hahn for LH cells and to Dr. C. Kane for continued advice in urologic oncology.

Supplementary materials

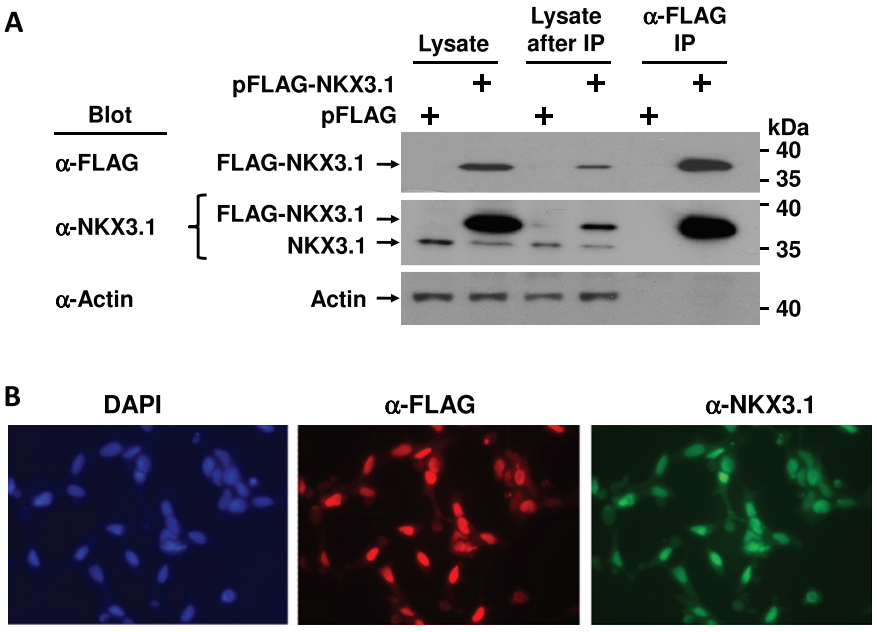

Figure S1. Transfection of FLAG-NKX3.1 expression into LNCaP cells and affinity purification. (**A**) LNCaP cells were transfected with pFLAG-NKX3.1 plasmid or with the empty pFLAG vector. Total cell lysate (lanes 1 and 2) was absorbed to anti-FLAG resin and eluted with FLAG peptides (lanes 5 and 6). The depleted cell lysate after affinity purification is shown in lanes 3 and 4. Immunoblots were probed with the indicated antibodies. The blot with NKX3.1 shows the overexpressed FLAG-NKX3.1 and the endogenous NKX3.1 protein (middle panel). Actin was used as loading reference. Cropped blot images are shown; see Figure S9 for full images. (**B**) LNCaP cells were transfected with pFLAG-NKX3.1 plasmid, and FLAG-NKX3.1 was detected by indirect immunofluorescence staining with FLAG or NKX3.1 antibodies.

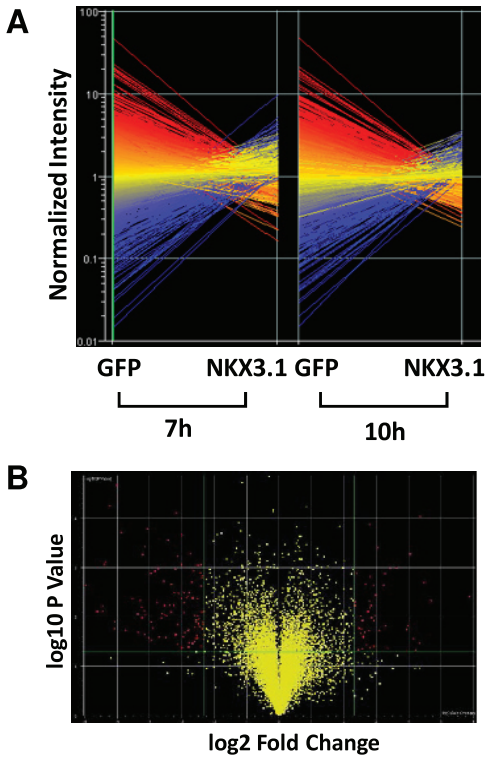

Figure S2. Global gene expression signature of NKX3.1 expression in LH cells. (**A**) Differential gene expression 7 and 10 h after NKX3.1 expression in LH cells. Note the overall similarity of gene expression differences between GFP and NKX3.1 expressing LH cells at both time points (7 h and 10 h). (**B**) "Volcano Plot" of differentially expressed genes at the 7 h time point. Features marked in red differed significantly 5-fold between GFP and NKX3.1 expressing samples.

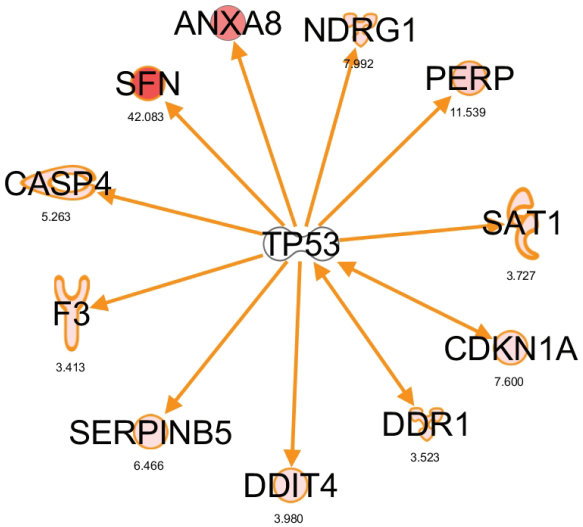

Figure S3. p53-linked expression changes. IPA-based rendering of mRNAs contained in the 5× datasets that were previously shown to be regulated by p53.

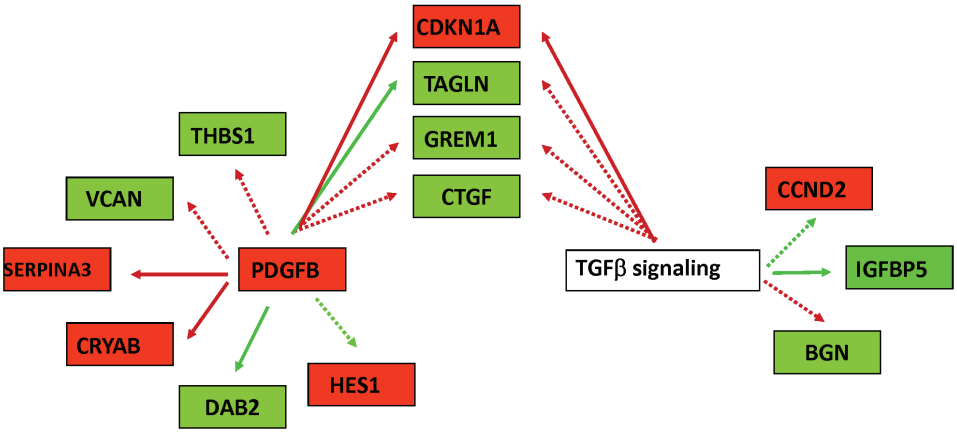

Figure S4. Schematic depiction of PDGFB and TGFβ expression edges according to IPA and comparison with the actual behavior of first degree nodes in response to NKX3.1 expression in LH cells. Green color indicates upregulation, whereas red color signifies downregulation. The arrows represent the expression edges. Solid arrows indicate agreement between observed expression behavior and the behavior expected in response to activation of PDFGB or TGFβ according to the information contained in the IPA database. The stippled arrows indicate disagreement. Example: PDGF is expected to upregulate HES1. Induction of PDGF by NKX3.1 is therefore consistent with the change in HES1 mRNA (edge is solid red arrow). PDGFB is also expected to upregulate THBS1 (red edge), but NKX3.1 expression leads to suppression of THBS1. Hence the edge is a stippled arrow.

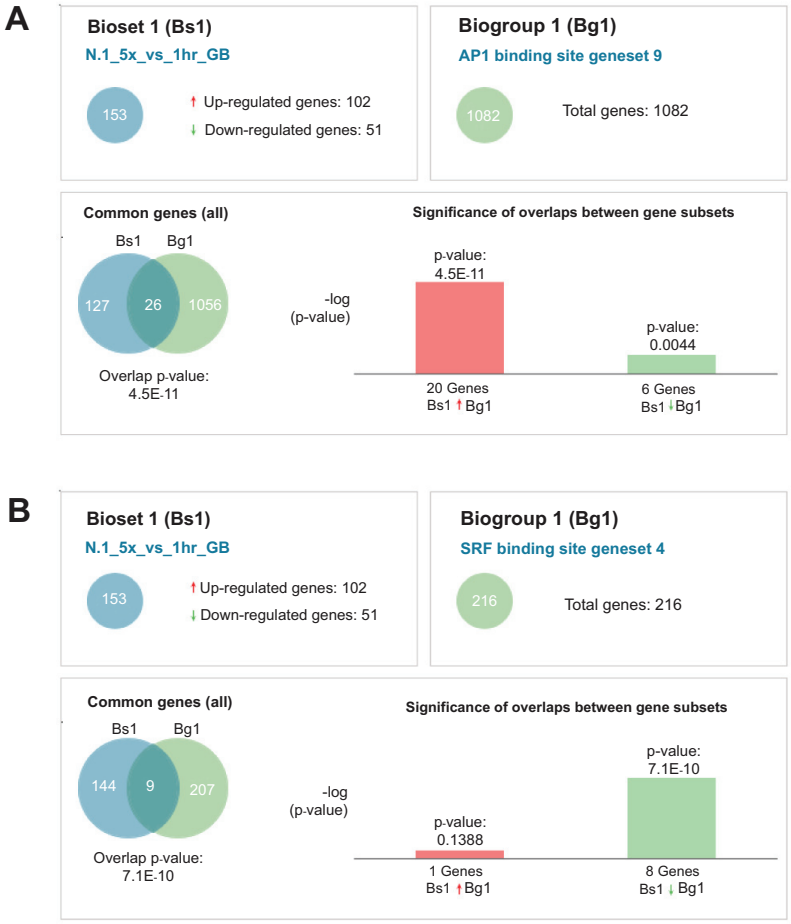

Figure S5. Enrichment of putative conserved AP1 and SRF binding sites in genes affected by NKX3.1 expression in LH cells as determined with NextBio. (**A**) The top panels summarize the datsets: Bioset 1 = 5× dataset of mRNAs affected by NKX3.1 expression; Biogroup 1 = AP1 binding site gene set according to[1]. The bottom panel illustrates the overlap between Bioset 1 and Biogroup 1 in a Venn diagram (left) and in bar graphs (right). The bar graph shows that most genes containing conserved AP1 binding sites are activated by NKX3.1 expression. The individual genes are indicated in Supplementary Table 1 and Supplementary Table 2. (**B**) Same as above for serum response factor (SRF).

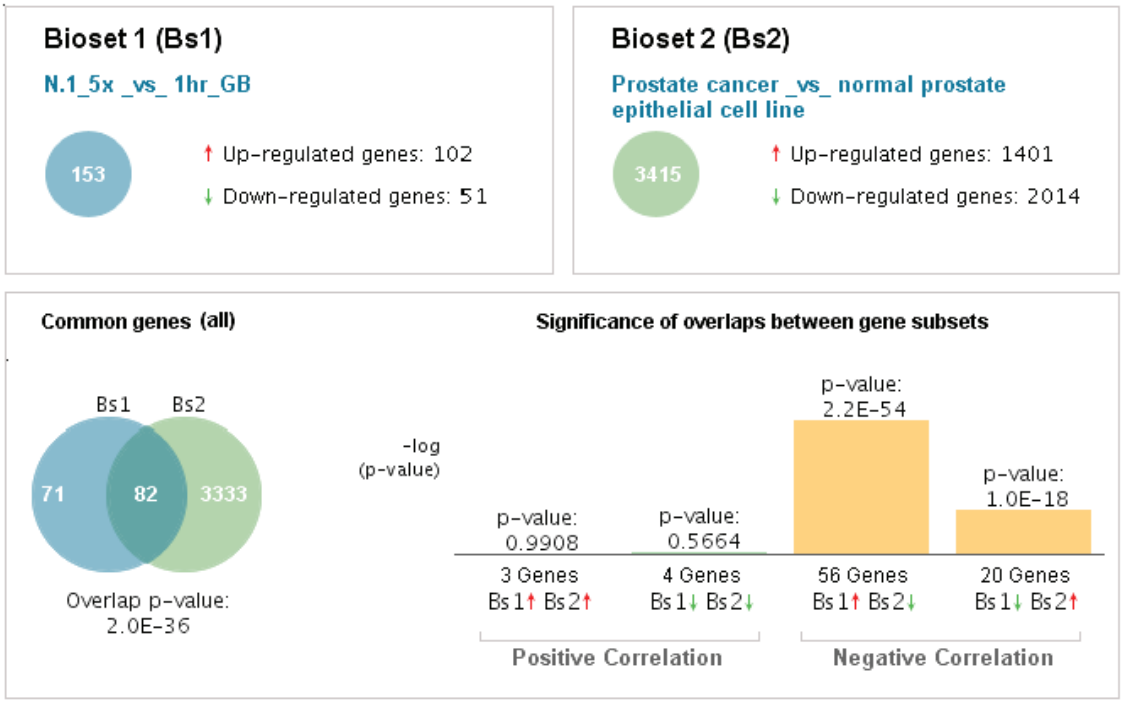

Figure S6. Overlap in mRNA expression between the 5× dataset and in human prostate cancer derived cell lines. (**A**) The top panels summarize the datasets: Bioset 1 = 5× dataset of mRNAs affected by NKX3.1 expression; Bioset 2 = Prostate cancer derived cell lines versus normal prostate epithelial cells[2]. The bottom panel illustrates the overlap between Bioset 1 and Bioset 2 in a Venn diagram (left) and in bar graphs (right). The bar graph highlights the largely opposite gene expression patterns in the two biosets. The individual genes are indicated in Supplementary Table 1 and Supplementary Table 2.

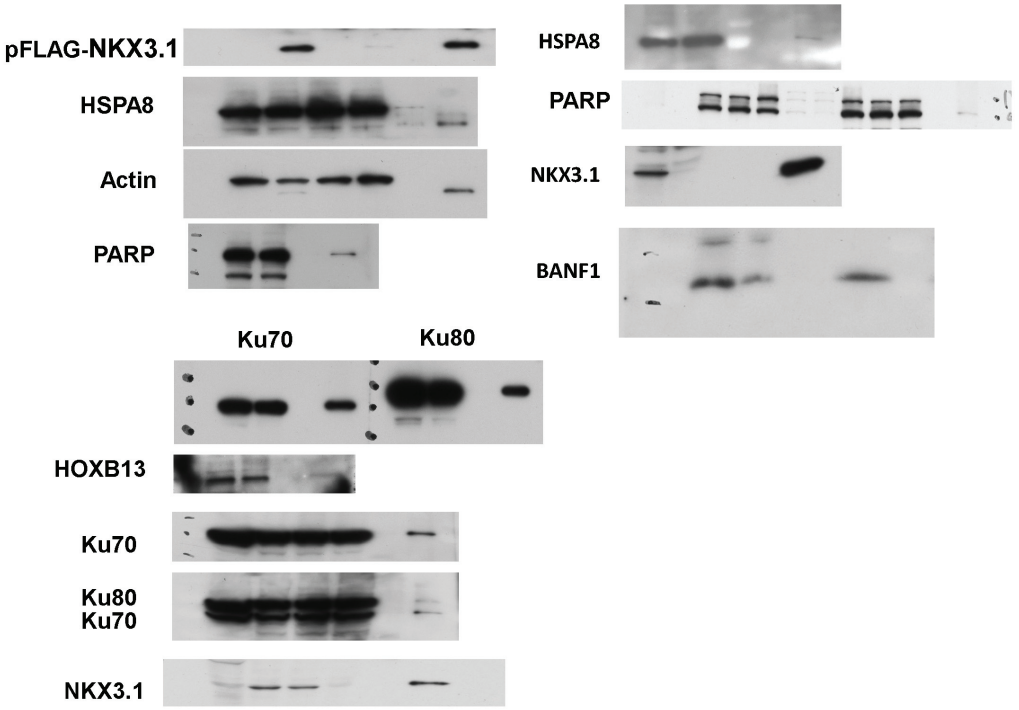

Figure S7. Uncropped immunoblots for Figure 2.

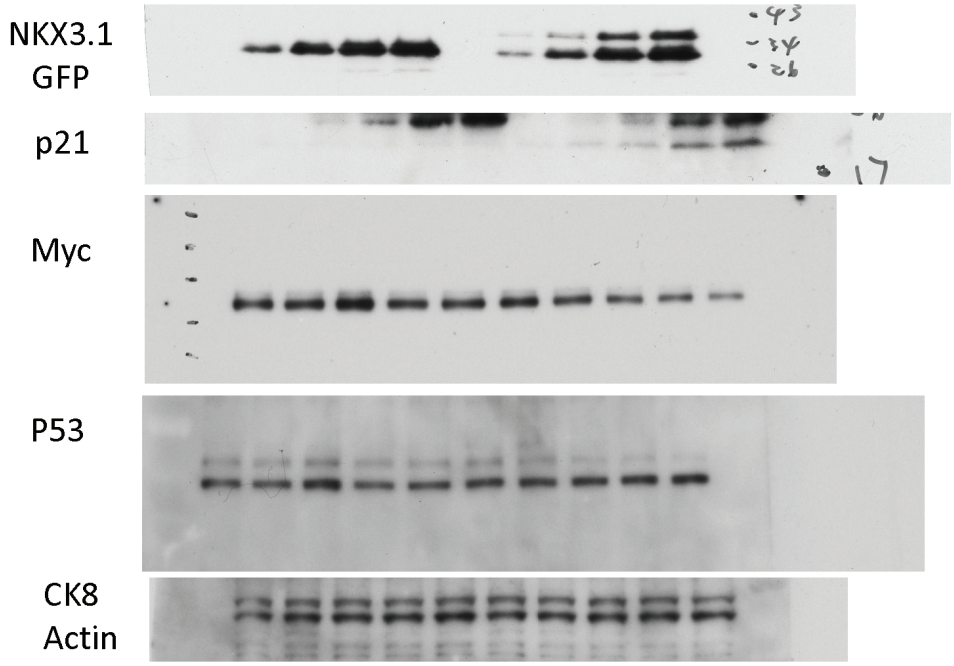

Figure S8. Uncropped immunoblots for Figure 6.

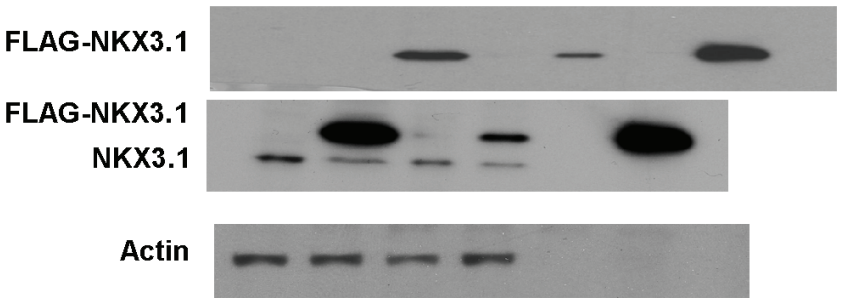

Figure S9. Uncropped immunoblots for Figure S1.

Supplementary Table 1 Genes upregulated in NKX3.1 overexpressing LH cells

GFP	NKX3.1	Fold Change	Common	Genbank	Description	PCa ↓ PCaDCL ↓AP1 SRF
95.81	6045.64	63.1	HSPA6	NM_002155.3	heat shock 70kDa protein 6 (HSP70B') (HSPA6)	
110.46	5468.87	49.5	KRT17	NM_000422.1	keratin 17 (KRT17)	
119.76	5346.03	44.6	S100A2	NM_005978.3	S100 calcium binding protein A2 (S100A2)	
93.23	4068.60	43.6	KRT5	NM_000424.2	keratin 5 (KRT5)	
93.98	3943.20	42.0	SFN	NM_006142.3	stratifin (SFN)	
97.80	4017.76	41.1	VAMP8	NM_003761.2	vesicle-associated membrane protein 8 (endobrevin) (VAMP8)	
97.57	3661.97	37.5	FGFBP1	NM_005130.3	fibroblast growth factor binding protein 1 (FGFBP1)	
107.32	3716.10	34.6	CCND2	NM_001759.2	cyclin D2 (CCND2)	
121.60	4128.94	34.0	LAMA3	NM_198129.1	laminin, alpha 3 (LAMA3), transcript variant 1	
88.46	2837.16	32.1	KRT19	NM_002276.3	keratin 19 (KRT19)	
144.93	4255.85	29.4	COL17A1	NM_130778.1	collagen, type XVII, alpha 1 (COL17A1), transcript variant short	
145.78	3897.20	26.7	SPINT2	NM_021102.2	serine peptidase inhibitor, Kunitz type, 2 (SPINT2)	
115.19	2687.88	23.3	ANXA8	NM_001630.1	annexin A8 (ANXA8)	
105.01	2180.30	20.8	SCNN1A	NM_001038.4	sodium channel, nonvoltage-gated 1 alpha (SCNN1A)	
101.89	2069.73	20.3	GNA15	NM_002068.1	guanine nucleotide binding protein (G protein), alpha 15 (Gq class) (GNA15)	
89.10	1728.43	19.4	C19orf33	NM_033520.1	chromosome 19 open reading frame 33 (C19orf33)	
107.32	2049.15	19.1	KRT6B	NM_005555.2	keratin 6B (KRT6B)	
103.83	1977.70	19.0	S100A14	NM_020672.1	S100 calcium binding protein A14 (S100A14)	
101.98	1897.81	18.6	HTRA1	NM_002775.3	HtrA serine peptidase 1 (HTRA1)	
117.36	2140.41	18.2	ALDH1A3	NM_000693.1	aldehyde dehydrogenase 1 family, member A3 (ALDH1A3)	
109.01	1977.00	18.1	SOX15	NM_006942.1	SRY (sex determining region Y)-box 15 (SOX15)	
100.36	1788.35	17.8	CLDN7	NM_001307.3	claudin 7 (CLDN7)	
100.53	1756.72	17.5	FEZ1	NM_005103.3	fasciculation and elongation protein zeta 1 (zygin I) (FEZ1), transcript variant 1	
93.82	1557.91	16.6	PRSS8	NM_002773.2	protease, serine, 8 (prostasin) (PRSS8)	
117.23	1908.68	16.3	DLL1	NM_005618.2	delta-like 1 (Drosophila) (DLL1)	
87.68	1366.63	15.6	CDH3	NM_001793.3	cadherin 3, type 1, P-cadherin (placental) (CDH3)	
108.56	1690.53	15.6	SERPINA3	NM_001085.4	serpin peptidase inhibitor member 3 (SERPINA3)	
120.16	1838.50	15.3	LAD1	NM_005558.3	ladinin 1 (LAD1)	
154.01	2268.36	14.7	LOC649970	XM_939056.1	PREDICTED: similar to creatine kinase, mitochondrial 1B precursor (LOC649970)	
179.94	2561.59	14.2	DNAJA4	NM_018602.2	DnaJ (Hsp40) homolog, subfamily A, member 4 (DNAJA4)	
111.14	1523.41	13.7	SH3PXD2A	NM_014631.2	SH3 and PX domains 2A (SH3PXD2A)	
127.84	1741.38	13.6	JUP	NM_021991.1	junction plakoglobin (JUP), transcript variant 2	
161.68	2091.77	12.9	CYGB	NM_134268.3	cytoglobin (CYGB)	
97.49	1212.63	12.4	SLPI	NM_003064.2	secretory leukocyte peptidase inhibitor (SLPI)	
106.40	1300.93	12.2	TNF	NM_000594.2	tumor necrosis factor (TNF superfamily, member 2) (TNF)	
138.73	1643.40	11.8	CRYAB	NM_001885.1	crystallin, alpha B (CRYAB)	
111.78	1315.18	11.8	PERP	NM_022121.2	PERP, TP53 apoptosis effector (PERP)	
98.74	1138.99	11.5	GJB2	NM_004004.3	gap junction protein, beta 2, 26kDa (connexin 26) (GJB2)	
93.66	1050.45	11.2	RAB25	NM_020387.1	RAB25, member RAS oncogene family (RAB25)	
132.86	1485.78	11.2	ALDOC	NM_005165.2	aldolase C, fructose-bisphosphate (ALDOC)	
114.30	1254.82	11.0	CKMT1A	NM_00101500	creatine kinase, mitochondrial 1A (CKMT1A), nuclear gene encoding mitochondrial protein	
102.38	1073.89	10.5	C10orf116	NM_006829.2	chromosome 10 open reading frame 116 (C10orf116)	
101.20	1032.76	10.2	SAA1	NM_199161.1	serum amyloid A1 (SAA1), transcript variant 2	
1144.71	11534.71	10.1	HSPA1A	NM_005345.4	heat shock 70kDa protein 1A (HSPA1A)	
105.70	1004.56	9.5	FLJ34922	NM_152270.2	likely ortholog of mouse schlafen 8/9 (FLJ34922)	
144.26	1370.50	9.5	SERINC2	NM_178865.3	serine incorporator 2 (SERINC2)	
152.90	1405.69	9.2	ITGB4	NM_00100561	integrin, beta 4 (ITGB4), transcript variant 2	
129.40	1180.33	9.1	MGST1	NM_020300.3	microsomal glutathione S-transferase 1 (MGST1), transcript variant 1b	
78.62	712.68	9.1	CA2	NM_000067.1	carbonic anhydrase II (CA2)	
128.99	1167.18	9.0	LAMC2	NM_018891.1	laminin, gamma 2 (LAMC2), transcript variant 2	
103.78	923.38	8.9	TACSTD1	NM_002354.1	tumor-associated calcium signal transducer 1 (TACSTD1)	
222.88	1936.09	8.7	CAMK2N1	NM_018584.4	calcium/calmodulin-dependent protein kinase II inhibitor 1 (CAMK2N1)	
438.21	3779.90	8.6	LAMA5	NM_005560.3	laminin, alpha 5 (LAMA5)	
89.45	768.40	8.6	CRABP2	NM_001878.2	cellular retinoic acid binding protein 2 (CRABP2)	
124.94	1032.32	8.3	C10orf10	NM_007021.2	chromosome 10 open reading frame 10 (C10orf10)	
105.80	866.72	8.2	CST6	NM_001323.2	cystatin E/M (CST6)	
122.14	998.28	8.2	MGC59937	NM_199001.1	Similar to RIKEN cDNA 2310002J15 gene (MGC59937)	
210.97	1687.56	8.0	NDRG1	NM_006096.2	N-myc downstream regulated gene 1 (NDRG1)	
132.68	1045.61	7.9	SAA1	NM_000331.2	serum amyloid A1 (SAA1), transcript variant 1	
94.15	732.60	7.8	OVOL2	NM_021220.2	ovo-like 2 (Drosophila) (OVOL2)	
189.75	1449.30	7.6	C3	NM_000064.1	complement component 3 (C3)	
141.54	1078.53	7.6	HES1	NM_005524.2	hairy and enhancer of split 1, (Drosophila) (HES1)	
524.45	3993.87	7.6	CDKN1A	NM_078467.1	cyclin-dependent kinase inhibitor 1A (p21, Cip1) (CDKN1A), transcript variant 2	
402.25	3054.38	7.6	DNAJB1	NM_006145.1	DnaJ (Hsp40) homolog, subfamily B, member 1 (DNAJB1)	
99.55	727.48	7.3	LOC652846	XM_942545.1	PREDICTED: similar to Annexin A8 (Annexin VIII) (Vascular anticoagulant-beta) mRNA.	
120.22	855.41	7.1		AF432419	C75F mRNA, complete cds	
106.48	750.63	7.0	LOC652878	XM_942594.1	PREDICTED: similar to heat shock 70kDa protein 6 (HSP70B) (LOC652878)	
98.31	689.97	7.0	JAG2	NM_002226.3	jagged 2 (JAG2), transcript variant 1	
108.89	757.99	7.0	KLK5	NM_012427.3	kallikrein 5 (KLK5)	
115.40	794.52	6.9	RASD1	NM_016084.3	RAS, dexamethasone-induced 1 (RASD1)	
449.41	3093.93	6.9	TFPI2	NM_006528.2	tissue factor pathway inhibitor 2 (TFPI2)	
104.51	704.84	6.7	MGC61598	XM_939432.1	PREDICTED: similar to ankyrin-repeat protein Nrarp (MGC61598)	
107.73	707.28	6.6	SERPINB5	NM_002639.2	serpin peptidase inhibitor, clade B (ovalbumin), member 5 (SERPINB5)	
95.91	615.45	6.4	IL1A	NM_000575.3	interleukin 1, alpha (IL1A)	
104.82	672.27	6.4	LCN2	NM_005564.2	lipocalin 2 (oncogene 24p3) (LCN2)	
95.65	605.92	6.3		DN919451	MCF7RNAL26H10TF; cDNA clone MCF7_RNA_L_26_H10, mRNA sequence	
166.88	1039.66	6.2	STK32B	NM_018401.1	serine/threonine kinase 32B (STK32B)	
90.80	554.44	6.1	GJB3	NM_00100573	gap junction protein, beta 3, 31kDa (connexin 31) (GJB3), transcript variant 2	
196.85	1192.45	6.1	PYCARD	NM_145183.1	PYD and CARD domain containing (PYCARD), transcript variant 3	
1796.87	10861.73	6.0	HSPA1B	NM_005346.3	heat shock 70kDa protein 1B (HSPA1B)	
102.67	619.47	6.0	MAL2	NM_052886.1	mal, T-cell differentiation protein 2 (MAL2)	
103.19	614.70	6.0	CD14	NM_000591.1	CD14 antigen (CD14)	
156.19	924.35	5.9	C1orf130	NM_00101098	chromosome 1 open reading frame 130 (C1orf130)	
252.76	1474.02	5.8	GPR56	NM_201525.1	G protein-coupled receptor 56 (GPR56), transcript variant 3	
165.69	950.47	5.7	GALNAC4S-6	NM_015892.2	B cell RAG associated protein (GALNAC4S-6ST)	
1465.73	8400.42	5.7	MT1X	NM_005952.2	metallothionein 1X (MT1X)	
174.41	995.86	5.7	RXRA	NM_002957.3	retinoid X receptor, alpha (RXRA)	
192.07	1095.07	5.7	ARHGEF16	NM_014448.2	Rho guanine exchange factor (GEF) 16 (ARHGEF16)	
84.77	482.18	5.7	SNX10	NM_013322.2	sorting nexin 10 (SNX10)	
161.59	908.48	5.6	TPD52L1	NM_00100339	tumor protein D52-like 1 (TPD52L1), transcript variant 3	
100.06	554.67	5.5	CKMT1B	NM_020990.3	creatine kinase, mitochondrial 1B (CKMT1B), nuclear gene encoding mitochondrial protein	
78.90	435.00	5.5	TMEM30B	NM_00101797	transmembrane protein 30B (TMEM30B)	
75.90	413.88	5.5	COL17A1	NM_000494.2	collagen, type XVII, alpha 1 (COL17A1), transcript variant long	
116.28	629.60	5.4	CYP27B1	NM_000785.3	cytochrome P450, family 27, (CYP27B1), nuclear gene encoding mitochondrial protein	
89.61	481.15	5.4	PADI3	NM_016233.1	peptidyl arginine deiminase, type III (PADI3)	
103.59	551.70	5.3	TNFRSF6B	NM_003823.2	tumor necrosis factor receptor superfamily, member 6b, decoy (TNFRSF6B)	
141.20	746.41	5.3	CASP4	NM_033306.2	caspase 4, apoptosis-related cysteine peptidase (CASP4), transcript variant gamma	
105.73	558.55	5.3	ADAM8	NM_001109.2	ADAM metallopeptidase domain 8 (ADAM8)	
620.09	3247.84	5.2	KRT7	NM_005556.3	keratin 7 (KRT7)	
71.65	373.96	5.2	SGPP2	XM_938742.1	PREDICTED: sphingosine-1-phosphate phosphotase 2 (SGPP2)	
145.03	750.85	5.2	VTI1A	NM_145206.1	vesicle transport through interaction with t-SNAREs homolog 1A (yeast) (VTI1A)	
248.33	1280.59	5.2	DMKN	NM_033317.2	dermokine (ZD52F10), transcript variant 2	
120.28	616.42	5.1	PDGFB	NM_033016.1	platelet-derived growth factor beta polypeptide (PDGFB), transcript variant 2	
92.53	470.15	5.1	FAM83A	NM_032899.4	family with sequence similarity 83, member A (FAM83A), transcript variant 1	
129.03	654.21	5.1	PANX2	NM_052839.2	pannexin 2 (PANX2)	
265.21	1335.89	5.0	GSTO2	NM_183239.1	glutathione S-transferase omega 2 (GSTO2)	
74.51	367.32	4.9	C20orf42	NM_017671.3	chromosome 20 open reading frame 42 (C20orf42)	

Red numbers indicate fold upregulation, green fields indicate downregulation, black fields indicate the presence of binding sites for the indicated transcription factors, Pca = prostate cancer; PCaDLC = Prostate cancer derived cell line; AP1 = Activator protein 1; SRF = Serum response factor

Supplementary Table 2 Genes downregulated in NKX3.1 overexpressing LH cells

GFP	NKX3.1	Fold Change	Common	Genbank	Description	PCa ↑	PCaDCL ↑	AP1	SRF
20346.20	346.53	-58.7	TAGLN	NM_003186.3	transgelin (TAGLN), transcript variant 2				
8558.84	332.86	-25.7	EEF1A2	NM_001958.2	eukaryotic translation elongation factor 1 alpha 2 (EEF1A2)				
2350.29	102.48	-22.9	GREM1	NM_013372.5	gremlin 1, (GREM1) BMP antagonist				
2729.31	133.15	-20.5	CDH2	NM_001792.2	cadherin 2, type 1, N-cadherin (neuronal) (CDH2)				
4163.75	203.80	-20.4	FOXD1	NM_004472.1	forkhead box D1 (FOXD1)				
4763.13	250.86	-19.0	FLNC	NM_001458.2	filamin C, gamma (actin binding protein 280) (FLNC)				
1685.00	91.27	-18.5	KISS1	NM_002256.2	KiSS-1 metastasis-suppressor (KISS1)				
2828.77	170.25	-16.6	H2BFS	NM_017445.1	H2B histone family, member S (H2BFS)				
1669.36	101.83	-16.4	COL5A1	NM_000093.2	collagen, type V, alpha 1 (COL5A1)				
2023.86	124.73	-16.2	COL1A1	NM_000088.2	collagen, type I, alpha 1 (COL1A1)				
1511.79	95.23	-15.9	IGFBP5	NM_000599.2	insulin-like growth factor binding protein 5 (IGFBP5)				
1245.24	98.50	-12.6	DKK1	NM_012242.2	dickkopf homolog 1 (Xenopus laevis) (DKK1)				
9981.32	926.93	-10.8	HIST1H2BK	NM_080593.1	histone 1, H2bk (HIST1H2BK)				
1898.60	183.20	-10.4	MYL9	NM_006097.3	myosin, light polypeptide 9, regulatory (MYL9), transcript variant 1				
866.92	87.80	-9.9	ANKRD1	NM_014391.2	ankyrin repeat domain 1 (cardiac muscle) (ANKRD1)				
3012.22	312.13	-9.7	UCHL1	NM_004181.3	ubiquitin carboxyl-terminal esterase L1 (ubiquitin thiolesterase) (UCHL1)				
1191.03	125.97	-9.5	FLJ90166	NM_153360.1	hypothetical protein FLJ90166 (FLJ90166)				
2731.68	320.47	-8.5	HIST1H1C	NM_005319.3	histone 1, H1c (HIST1H1C)				
1386.94	167.25	-8.3	C21orf7	NM_020152.2	chromosome 21 open reading frame 7 (C21orf7)				
734.37	91.82	-8.0	HAK	NM_052947.2	heart alpha-kinase (HAK)				
1119.88	143.28	-7.8	SAMD9L	NM_152703.2	sterile alpha motif domain containing 9-like (SAMD9L)				
2827.18	362.56	-7.8	IFIT3	NM_001549.2	interferon-induced protein with tetratricopeptide repeats 3 (IFIT3)				
4915.30	638.92	-7.7	TPM1	NM_000366.5	tropomyosin 1 (alpha) (TPM1), transcript variant 5				
1592.98	210.41	-7.6	CRIP1	NM_001311.3	cysteine-rich protein 1 (intestinal) (CRIP1)				
1899.13	252.10	-7.5	ZNFX1	NM_021035.1	zinc finger, NFX1-type containing 1 (ZNFX1)				
860.45	117.66	-7.3	HIST1H2AC	NM_003512.3	histone 1, H2ac (HIST1H2AC)				
1254.04	173.13	-7.2	COL5A2	NM_000393.2	collagen, type V, alpha 2 (COL5A2)				
745.48	103.08	-7.2	CSPG2	NM_004385.2	chondroitin sulfate proteoglycan 2 (versican) (CSPG2)				
926.98	131.84	-7.0	HIST1H2BD	NM_138720.1	histone 1, H2bd (HIST1H2BD), transcript variant 2				
659.60	94.04	-7.0	BGN	NM_001711.3	biglycan (BGN)				
4342.70	631.33	-6.9	CTGF	NM_001901.1	connective tissue growth factor (CTGF)				
3043.84	442.85	-6.9	TNC	NM_002160.1	tenascin C (hexabrachion) (TNC)				
5592.26	814.41	-6.9	IFI35	NM_005533.2	interferon-induced protein 35 (IFI35)				
1098.59	164.59	-6.7	HRASLS3	NM_007069.1	HRAS-like suppressor 3 (HRASLS3)				
8826.28	1335.18	-6.6	TAP1	NM_000593.5	transporter 1, ATP-binding cassette, sub-family B (MDR/TAP) (TAP1)				
1024.41	161.62	-6.3	TNFSF10	NM_003810.2	tumor necrosis factor (ligand) superfamily, member 10 (TNFSF10)				
1271.92	203.46	-6.3	DAB2	NM_001343.1	disabled homolog 2, mitogen-responsive phosphoprotein (Drosophila) (DAB2)				
571.48	92.78	-6.2	SIM2	NM_005069.2	single-minded homolog 2 (Drosophila) (SIM2), transcript variant SIM2				
1556.36	256.03	-6.1	TRIM22	NM_006074.2	tripartite motif-containing 22 (TRIM22)				
5505.46	906.28	-6.1	RAGE	NM_014226.1	renal tumor antigen (RAGE)				
4791.61	788.84	-6.1	STAT2	NM_005419.2	signal transducer and activator of transcription 2, 113kDa (STAT2)				
676.57	112.59	-6.0	NPTX1	NM_002522.2	neuronal pentraxin I (NPTX1)				
4485.08	750.68	-6.0	KLF6	NM_001300.4	Kruppel-like factor 6 (KLF6), transcript variant 2				
4408.67	764.67	-5.8	THBS1	NM_003246.2	thrombospondin 1 (THBS1)				
2424.90	422.90	-5.7	IFI44L	NM_006820.1	interferon-induced protein 44-like (IFI44L)				
888.14	155.10	-5.7	OXTR	NM_000916.3	oxytocin receptor (OXTR)				
596.39	104.82	-5.7	ACTG2	NM_001615.3	actin, gamma 2, smooth muscle, enteric (ACTG2)				
1850.60	338.21	-5.5	THY1	NM_006288.2	Thy-1 cell surface antigen (THY1)				
615.68	116.02	-5.3	MYLK	NM_005965.3	myosin, light polypeptide kinase (MYLK), transcript variant 6				
705.08	138.13	-5.1	C2orf32	NM_015463.1	chromosome 2 open reading frame 32 (C2orf32)				
2339.28	461.31	-5.1	PLEKHC1	NM_006832.1	pleckstrin homology domain containing, family C member 1 (PLEKHC1)				

Green numbers indicate fold downregulation, red fields indicate upregulation, black fields indicate the presence of binding sites for the indicated transcription factors; Pca = prostate cancer; PCaDLC = Prostate cancer derived cell line; AP1 = Activator protein 1; SRF = Serum response factor

Supplementary Table 3 Overlap between NKX3.1 target genes in mouse and in human cells

Human ID	Human Symbol	Entrez Gene Description	Regulation by NKX3.1 in human cells	Mouse Symbol	Regulation by NKX3.1 in mice
NM_000067.1	CA2	carbonic anhydrase II	Activated	Car2	Activated
NM_019058.2	DDIT4	DNA-damage-inducible transcript 4	Activated	Ddit4	Activated
NM_002155.3	HSPA6	heat shock 70kDa protein 6 (HSP70B')	Activated	Hspa5	Activated
NM_005950.1	MT1G	metallothionein 1G	Activated	Mt1	Activated
NM_005952.2	MT1X	metallothionein 1X	Activated	Mt1	Activated
NM_033381.1	COL4A5	collagen, type IV, alpha 5	Activated	Col4a5	Repressed
NM_014988.1	LIMCH1	LIM and calponin homology domains 1	Repressed	Limch1	Activated
NM_153360.1	APCDD1L	adenomatosis polyposis coli down-regulated 1-like	Repressed	Apcdd1	Repressed
NM_152330.2	FRMD6	FERM domain containing 6	Repressed	Frmd6	Repressed
NM_006472.1	TXNIP	thioredoxin interacting protein	Repressed	Txnip	Repressed

Ref.: Anderson et al. Journal of Clinical Investigation 2012, 122:1907–1919.

Supplementary Table 4 Predicted and actual response to TGFα and NKX3.1

Name	TGFα response predicted by expression edge	Actual response to NKX3.1
LAMA3	↑	↑
ALDH1A3	↑	↑
LAD1	↑	↑
SAA1	↑	↑
HSPA1A	↑	↑
LAMC2	↑	↑
C10orf10	↑	↑
JAG2	↑	↑
TFPI2	↑	↑
LCN2	↑	↑
CD14	↑	↑
CASP4	↑	↑
ADAM8	↑	↑
PDGFB	↑	↑
RASD1	↓	↑
MGST1	↓	↑
IFIT3	↑	↓
MYLK	↑	↓

Supplementary Table 5 Control of TGFβ-related gene expression by NKX3.1

GFP	NKX3.1	Fold Change	Common Name	Desciption
901.3701	201.12804	-4.481573529	TGFB1I1	transforming growth factor beta 1 induced transcript 1 (TGFB1I1)
339.3748	85.09652	-3.988116083	TGFB2	transforming growth factor, beta 2 (TGFB2)
531.43066	237.8984	-2.233855545	TGFBR2	transforming growth factor, beta receptor II (70/80kDa) (TGFBR2), transcript variant 1
337.46625	158.84158	-2.124546041	SMAD7	SMAD, mothers against DPP homolog 7 (Drosophila) (SMAD7)
3151.0513	1573.5414	-2.002522018	TGFBI	transforming growth factor, beta-induced, 68kDa (TGFBI)
209.2047	126.932335	-1.648159234	TGFBRAP1	transforming growth factor, beta receptor associated protein 1 (TGFBRAP1)
638.00244	389.01108	-1.640062386	TGIF2	TGFB-induced factor 2 (TALE family homeobox) (TGIF2)
125.47178	85.58007	-1.466133178	SMAD6	SMAD, mothers against DPP homolog 6 (Drosophila) (SMAD6)
677.43225	504.6805	-1.342299237	SMAD4	SMAD, mothers against DPP homolog 4 (Drosophila) (SMAD4)
118.65842	89.9339	-1.319395912	TGIF	TGFB-induced factor (TALE family homeobox) (TGIF), transcript variant 2
386.59677	302.59946	-1.277585789	SNIP1	Smad nuclear interacting protein 1 (SNIP1)
133.12515	107.34483	-1.240163592	SMURF2	SMAD specific E3 ubiquitin protein ligase 2 (SMURF2)
396.22388	322.08224	-1.230194748	SMAD3	SMAD, mothers against DPP homolog 3 (Drosophila) (SMAD3)
110.44686	90.07587	-1.226153686	TGIF	TGFB-induced factor (TALE family homeobox) (TGIF), transcript variant 4
119.22626	97.336044	-1.224893216	TGFBR3	transforming growth factor, beta receptor III (betaglycan, 300kDa) (TGFBR3)
321.90323	267.21222	-1.204672563	TGIF	TGFB-induced factor (TALE family homeobox) (TGIF), transcript variant 1
209.43947	186.34435	-1.12393786	SMURF1	SMAD specific E3 ubiquitin protein ligase 1 (SMURF1), transcript variant 2
114.60477	102.95182	-1.113188383	LOC653804	similar to SMAD, mothers against DPP homolog 2 (Drosophila) (LOC653804)
141.06203	133.9327	-1.05323069	SMAD2	SMAD, mothers against DPP homolog 2 (Drosophila) (SMAD2), transcript variant 2
135.20764	131.16252	-1.030840518	TGFBR1	transforming growth factor, beta receptor I (TGFBR1)
114.35846	111.279144	-1.027671996	TGFB1	transforming growth factor, beta 1 (TGFB1)
106.51333	105.51177	-1.009492401	SMAD1	SMAD, mothers against DPP homolog 1 (Drosophila) (SMAD1), transcript variant 2
106.71678	118.3267	1.108791888	TAIP-2	TGF-beta induced apotosis protein 2 (TAIP-2)
425.55972	510.4316	1.199435886	SMAD5	SMAD, mothers against DPP homolog 5 (Drosophila) (SMAD5), transcript variant 1
1211.3107	1468.2693	1.212132692	TINP1	TGF beta-inducible nuclear protein 1 (TINP1)

mRNAs downregulated >1.5-fold

Supplementary Table 6 Raw hybridization values for TNFSF10/TRAIL of duplicate samples

	GFP				NKX3.1			
	7 h		10h		7h		10h	
TNFSF10/T	1058.53	990.92	1076.59	1139.69	169.59	153.63	168.56	132.50

References

1. Xie, X. *et al.* Systematic discovery of regulatory motifs in human promoters and 3' UTRs by comparison of several mammals. *Nature* **434**, 338–345 (2005).

2. Nanni, S. *et al.* Epithelial-Restricted Gene Profile of Primary Cultures from Human Prostate Tumors: A Molecular Approach to Predict Clinical Behavior of Prostate Cancer. *Molecular Cancer Research* **4**, 79 –92 (2006).

References

1. Abate-Shen C, Shen MM, Gelmann E: **Integrating differentiation and cancer: the Nkx3.1 homeobox gene in prostate organogenesis and carcinogenesis.** *Differentiation.* 2008; **76**(6): 717–27.
PubMed Abstract | Publisher Full Text | Free Full Text

2. Shen MM, Abate-Shen C: **Roles of the Nkx3.1 homeobox gene in prostate organogenesis and carcinogenesis.** *Dev Dyn.* 2003; **228**(4): 767–78.
PubMed Abstract | Publisher Full Text

3. Bhatia-Gaur R, Donjacour AA, Sciavolino PJ, *et al.*: **Roles for Nkx3.1 in prostate development and cancer.** *Genes Dev.* 1999; **13**(8): 966–77.
PubMed Abstract | Free Full Text

4. Tanaka M, Komuro I, Inagaki H, *et al.*: **Nkx3.1, a murine homolog of Ddrosophila bagpipe, regulates epithelial ductal branching and proliferation of the prostate and palatine glands.** *Dev Dyn.* 2000; **219**(2): 248–60.
PubMed Abstract

5. Kim MJ, Bhatia-Gaur R, Banach-Petrosky WA, *et al.*: **Nkx3.1 mutant mice recapitulate early stages of prostate carcinogenesis.** *Cancer Res.* 2002; **62**(11): 2999–3004.
PubMed Abstract

6. Abdulkadir SA, Magee JA, Peters TJ, *et al.*: **Conditional loss of Nkx3.1 in adult mice induces prostatic intraepithelial neoplasia.** *Mol Cell Biol.* 2002; **22**(5): 1495–503.
PubMed Abstract | Publisher Full Text | Free Full Text

7. Gary B, Azuero R, Mohanty GS, *et al.*: **Interaction of Nkx3.1 and p27kip1 in prostate tumor initiation.** *Am J Pathol.* 2004; **164**(5): 1607–14.
PubMed Abstract | Publisher Full Text | Free Full Text

8. Kim MJ, Cardiff RD, Desai N, *et al.*: **Cooperativity of Nkx3.1 and Pten loss of function in a mouse model of prostate carcinogenesis.** *Proc Natl Acad Sci U S A.* 2002; **99**(5): 2884–9.
PubMed Abstract | Publisher Full Text | Free Full Text

9. Lei Q, Jiao J, Xin L, *et al.*: **NKX3.1 stabilizes p53, inhibits AKT activation, and blocks prostate cancer initiation caused by PTEN loss.** *Cancer Cell.* 2006; **9**(5): 367–78.
PubMed Abstract | Publisher Full Text

10. Bowen C, Bubendorf L, Voeller HJ, *et al.*: **Loss of NKX3.1 expression in human prostate cancers correlates with tumor progression.** *Cancer Res.* 2000; **60**(21): 6111–5.
PubMed Abstract

11. Steadman DJ, Giuffrida D, Gelmann EP: **DNA-binding sequence of the human prostate-specific homeodomain protein NKX3.1.** *Nucleic Acids Res.* 2000; **28**(12): 2389–95.
PubMed Abstract | Publisher Full Text | Free Full Text

12. Choi CY, Kim YH, Kwon HJ, *et al.*: **The homeodomain protein NK-3 recruits Groucho and a histone deacetylase complex to repress transcription.** *J Biol Chem.* 1999; **274**(47): 33194–7.
PubMed Abstract

13. Simmons SO, Horowitz JM: **Nkx3.1 binds and negatively regulates the transcriptional activity of Sp-family members in prostate-derived cells.** *Biochem J.* 2006; **393**(Pt 1): 397–409.
PubMed Abstract | Publisher Full Text | Free Full Text

14. Chen H, Nandi AK, Li X, *et al.*: **NKX-3.1 interacts with prostate-derived Ets factor and regulates the activity of the PSA promoter.** *Cancer Res.* 2002; **62**(2): 338–40.
PubMed Abstract

15. Liu W, Zhang P, Chen W, *et al.*: **Characterization of two functional NKX 3.1 binding sites upstream of the PCAN1 gene that are involved in the positive regulation of PCAN1 gene transcription.** *BMC Mol Biol.* 2008; **9**(1): 45.
PubMed Abstract | Publisher Full Text | Free Full Text

16. Anderson PD, McKissic SA, Logan M, *et al.*: **Nkx3.1 and Myc crossregulate shared target genes in mouse and human prostate tumorigenesis.** *J Clin Invest.* 2012; **122**(5): 1907–19.
PubMed Abstract | Publisher Full Text | Free Full Text

17. Carson JA, Fillmore RA, Schwartz RJ, *et al.*: **The smooth muscle gamma-actin gene promoter is a molecular target for the mouse bagpipe homologue, mNkx3-1, and serum response factor.** *J. Biol Chem.* 2000; **275**(50): 39061–72.
PubMed Abstract | Publisher Full Text

18. Tan PY, Chang CW, Chng KR, *et al.*: **Integration of regulatory networks by NKX3-1 promotes androgen-dependent prostate cancer survival.** *Mol Cell Biol.* 2012; **32**(2): 399–414.
PubMed Abstract | Publisher Full Text | Free Full Text

19. Magee JA, Abdulkadir SA, Milbrandt J: **Haploinsufficiency at the Nkx3.1 locus: A paradigm for stochastic, dosage-sensitive gene regulation during tumor initiation.** *Cancer Cell.* 2003; **3**(3): 273–83.
PubMed Abstract | Publisher Full Text

20. Ouyang X, DeWeese TL, Nelson WG, *et al.*: **Loss-of-function of Nkx3.1 promotes increased oxidative damage in prostate carcinogenesis.** *Cancer Res.* 2005; **65**(15): 6773–9.
PubMed Abstract | Publisher Full Text

21. Ju JH, Maeng JS, Zemedkun M, *et al.*: **Physical and functional interactions between the prostate suppressor homeoprotein NKX3.1 and serum response factor.** *J Mol Biol.* 2006; **360**(5): 989–99.
PubMed Abstract | Publisher Full Text

22. Bowen C, Stuart A, Ju JH, *et al.*: **NKX3.1 homeodomain protein binds to topoisomerase I and enhances its activity.** *Cancer Res.* 2007; **67**(2): 455–64.
PubMed Abstract | Publisher Full Text

23. Song L, Bowen C, Gelmann EP: **Structural and functional interactions of the prostate cancer suppressor protein NKX3.1 with topoisomerase I.** *Biochem J.* 2013; **453**(1): 125–36.
PubMed Abstract | Publisher Full Text

24. Bowen C, Gelmann EP: **NKX3.1 activates cellular response to DNA damage.** *Cancer Res.* 2010; **70**(8): 3089–97.
PubMed Abstract | Publisher Full Text

25. Berger R, Febbo PG, Majumder PK, *et al.*: **Androgen-induced differentiation and tumorigenicity of human prostate epithelial cells.** *Cancer Res.* 2004; **64**(24): 8867–8875.
PubMed Abstract | Publisher Full Text

26. Lu L, Schulz H, Wolf DA: **The F-box protein SKP2 mediates androgen control of p27 stability in LNCaP human prostate cancer cells.** *BMC Cell Biol.* 2002; **3**(1): 22.
PubMed Abstract | Publisher Full Text | Free Full Text

27. Brill LM, Motamedchaboki K, Wu S, *et al.*: **Comprehensive proteomic analysis of Schizosaccharomyces pombe by two-dimensional HPLC-tandem mass spectrometry.** *Methods.* 2009; **48**(3): 311–9.
PubMed Abstract | Publisher Full Text | Free Full Text

28. Sha Z, Brill LM, Cabrera R, *et al.*: **The eIF3 interactome reveals the translasome, a supercomplex linking protein synthesis and degradation machineries.** *Mol Cell.* 2009; **36**(1): 141–52.
PubMed Abstract | Publisher Full Text | Free Full Text

29. Liu H, Sadygov RG, Yates JR 3rd: **A model for random sampling and estimation of relative protein abundance in shotgun proteomics.** *Anal Chem.* 2004; **76**(14): 4193–201.
PubMed Abstract | Publisher Full Text

30. Keller A, Eng J, Zhang N, *et al.*: **A uniform proteomics MS/MS analysis platform utilizing open XML file formats.** *Mol Syst Biol.* 2005.
PubMed Abstract | Publisher Full Text | Free Full Text

31. Schmidt MW, Houseman A, Ivanov AR, *et al.*: **Comparative proteomic and transcriptomic profiling of the fission yeast Schizosaccharomyces pombe.** *Mol Syst Biol.* 2007; **3**: 79.
PubMed Abstract | Publisher Full Text | Free Full Text

32. Wu G, Feng X, Stein L: **A human functional protein interaction network and its application to cancer data analysis.** *Genome Biol.* 2010; **11**(5): R53.
PubMed Abstract | Publisher Full Text | Free Full Text

33. Gautier L, Cope L, Bolstad BM, *et al.*: **affy---analysis of Affymetrix GeneChip data at the probe level.** *Bioinformatics.* 2004; **20**(3): 307–315.
PubMed Abstract | Publisher Full Text

34. Nanni S, Priolo C, Grasselli A, *et al.*: **Epithelial-restricted gene profile of primary cultures from human prostate tumors: a molecular approach to predict clinical behavior of prostate cancer.** *Mol Cancer Res.* 2006; **4**(2): 79–92.
PubMed Abstract | Publisher Full Text

35. Li X, Guan B, Maghami S, *et al.*: **NKX3.1 is regulated by protein kinase CK2 in**

prostate tumor cells. *Mol Cell Biol.* 2006; **26**(8): 3008–17.
PubMed Abstract | Publisher Full Text | Free Full Text

36. Markowski MC, Bowen C, Gelmann EP: **Inflammatory cytokines induce phosphorylation and ubiquitination of prostate suppressor protein NKX3.1.** *Cancer Res.* 2008; **68**(17): 6896–901.
PubMed Abstract | Publisher Full Text | Free Full Text

37. Smith GC, Jackson SP: **The DNA-dependent protein kinase.** *Genes Dev.* 1999; **13**(8): 916–934.
PubMed Abstract

38. Giffin W, Torrance H, Rodda DJ, *et al.*: **Sequence-specific DNA binding by Ku autoantigen and its effects on transcription.** *Nature.* 1996; **380**(6571): 265–8.
PubMed Abstract | Publisher Full Text

39. Krishnakumar R, Kraus WL: **The PARP side of the nucleus: molecular actions, physiological outcomes, and clinical targets.** *Mol Cell.* 2010; **39**(1): 8–24.
PubMed Abstract | Publisher Full Text | Free Full Text

40. Schild-Poulter C, Pope L, Giffin W, *et al.*: **The binding of Ku antigen to homeodomain proteins promotes their phosphorylation by DNA-dependent protein kinase.** *J Biol Chem.* 2001; **276**(20): 16848–16856.
PubMed Abstract | Publisher Full Text

41. Ruscetti T, Lehnert BE, Halbrook J, *et al.*: **Stimulation of the DNA-dependent protein kinase by poly(ADP-ribose) polymerase.** *J Biol Chem.* 1998; **273**(23): 14461–14467.
PubMed Abstract

42. Erbaykent-Tepedelen B, Karamil S, Gonen-Korkmaz C, *et al.*: **DNA damage response (DDR) via NKX3.1 expression in prostate cells.** *J Steroid Biochem Mol Biol.* 2014; **141**: 26–36.
PubMed Abstract | Publisher Full Text

43. Ting NS, Kao PN, Chan DW, *et al.*: **DNA-dependent protein kinase interacts with antigen receptor response element binding proteins NF90 and NF45.** *J Biol Chem.* 1998; **273**(4): 2136–2145.
PubMed Abstract

44. Jønson L, Vikesaa J, Krogh A, *et al.*: **Molecular composition of IMP1 ribonucleoprotein granules.** *Mol Cell Proteomics.* 2007; **6**(5): 798–811.
PubMed Abstract | Publisher Full Text

45. Han SP, Tang YH, Smith R: **Functional diversity of the hnRNPs: past, present and perspectives.** *Biochem J.* 2010; **430**(3): 379–92.
PubMed Abstract | Publisher Full Text

46. Andersen JS, Lyon CE, Fox AH, *et al.*: **Directed proteomic analysis of the human nucleolus.** *Curr Biol* 2002; **12**(1): 1–11.
PubMed Abstract | Publisher Full Text

47. Scherl A, Coute Y, Deon C, *et al.*: **Functional proteomic analysis of human nucleolus.** *Mol Biol Cell.* 2002; **13**(11): 4100–9.
PubMed Abstract | Publisher Full Text | Free Full Text

48. Pandit S, Wang D, Fu XD: **Functional integration of transcriptional and RNA processing machineries.** *Curr Opin Cell Biol.* 2008; **20**(3): 260–5.
PubMed Abstract | Publisher Full Text | Free Full Text

49. Fang X, Yoon JG, Li L, *et al.*: **Landscape of the SOX2 protein-protein interactome.** *Proteomics.* 2011; **11**(5): 921–34.
PubMed Abstract | Publisher Full Text

50. Segura-Totten M, Wilson KL: **BAF: roles in chromatin, nuclear structure and retrovirus integration.** *Trends Cell Biol.* 2004; **14**(5): 261–6.
PubMed Abstract | Publisher Full Text

51. Wang X, Xu S, Rivolta C, *et al.*: **Barrier to autointegration factor interacts with the cone-rod homeobox and represses its transactivation function.** *J Biol Chem.* 2002; **277**(45): 43288–300.
PubMed Abstract | Publisher Full Text

52. Norris JD, Chang CY, Wittmann BM, *et al.*: **The homeodomain protein HOXB13 regulates the cellular response to androgens.** *Mol Cell.* 2009; **36**(3): 405–16.
PubMed Abstract | Publisher Full Text | Free Full Text

53. Ewing CM, Ray AM, Lange EM, *et al.*: **Germline mutations In HOXB13 and prostate-cancer risk.** *N Engl J Med.* 2012; **366**(2): 141–9.
PubMed Abstract | Publisher Full Text | Free Full Text

54. Wang XD, Leow CC, Zha J, *et al.*: **Notch signaling is required for normal prostatic epithelial cell proliferation and differentiation.** *Dev Biol.* 2006; **290**(1): 66–80.
PubMed Abstract | Publisher Full Text

55. Missero C, Calautti E, Eckner R, *et al.*: **Involvement of the cell-cycle inhibitor Cip1/WAF1 and the E1A-associated p300 protein in terminal differentiation.** *Proc Natl Acad Sci U S A.* 1995; **92**(12): 5451–5.
PubMed Abstract | Publisher Full Text | Free Full Text

56. Rehman I, Cross SS, Catto JW, *et al.*: **Promoter hyper-methylation of calcium binding proteins S100A6 and S100A2 in human prostate cancer.** *Prostate.* 2005; **65**(4): 322–30.
PubMed Abstract | Publisher Full Text

57. Lodygin D, Diebold J, Hermeking H: **Prostate cancer is characterized by epigenetic silencing of 14-3-3sigma expression.** *Oncogene.* 2004; **23**(56): 9034–41.
PubMed Abstract | Publisher Full Text

58. Urano T, Takahashi S, Suzuki T, *et al.*: **14-3-3sigma is down-regulated in human prostate cancer.** *Biochem Biophys Res Commun.* 2004; **319**(3): 795–800.
PubMed Abstract | Publisher Full Text

59. Sathyanarayana UG, Padar A, Suzuki M, *et al.*: **Aberrant promoter methylation of laminin-5-encoding genes in prostate cancers and its relationship to clinicopathological features.** *Clin Cancer Res.* 2003; **9**(17): 6395–400.
PubMed Abstract

60. Sheehan GM, Kallakury BV, Sheehan CE, *et al.*: **Loss of claudins-1 and -7 and expression of claudins-3 and -4 correlate with prognostic variables in prostatic adenocarcinomas.** *Hum Pathol.* 2007; **38**(4): 564–9.
PubMed Abstract | Publisher Full Text

61. Takahashi S, Suzuki S, Inaguma S, *et al.*: **Down-regulated expression of prostasin in high-grade or hormone-refractory human prostate cancers.** *Prostate.* 2003; **54**(3): 187–93.
PubMed Abstract | Publisher Full Text

62. Jarrard DF, Paul R, van Bokhoven A, *et al.*: **P-Cadherin is a basal cell-specific epithelial marker that is not expressed in prostate cancer.** *Clin Cancer Res.* 1997; **3**(11): 2121–8.
PubMed Abstract

63. Yousef GM, Scorilas A, Chang A, *et al.*: **Down-regulation of the human kallikrein gene 5 (KLK5) in prostate cancer tissues.** *Prostate.* 2002; **51**(2): 126–32.
PubMed Abstract | Publisher Full Text

64. Henrique R, Costa VL, Cerveira N, *et al.*: **Hypermethylation of Cyclin D2 is associated with loss of mRNA expression and tumor development in prostate cancer.** *J Mol Med (Berl).* 2006; **84**(11): 911–8.
PubMed Abstract | Publisher Full Text

65. Cornford PA, Dodson AR, Parsons KF, *et al.*: **Heat shock protein expression independently predicts clinical outcome in prostate cancer.** *Cancer Res.* 2000; **60**(24): 7099–7105.
PubMed Abstract

66. Wang MH, Grossmann ME, Young CY: **Forced expression of heat-shock protein 70 increases the secretion of Hsp70 and provides protection against tumour growth.** *Br J Cancer.* 2004; **90**(4): 926–31.
PubMed Abstract | Publisher Full Text | Free Full Text

67. Tomlinson V, Newbery H, Wray N, *et al.*: **Translation elongation factor eEF1A2 is a potential oncoprotein that is overexpressed in two-thirds of breast tumours.** *BMC Cancer.* 2005; **5**(1): 113.
PubMed Abstract | Publisher Full Text | Free Full Text

68. Namkoong H, Shin S, Kim H, *et al.*: **The bone morphogenetic protein antagonist gremlin 1 is overexpressed in human cancers and interacts with YWHAH protein.** *BMC Cancer.* 2006; **6**(1): 74.
PubMed Abstract | Publisher Full Text | Free Full Text

69. Katoh M, Katoh M: **Human FOX gene family (Review).** *Int J Oncol.* 2004; **25**(5): 1495–500.
PubMed Abstract | Publisher Full Text

70. Jaggi M, Nazemi T, Abrahams NA, *et al.*: **N-cadherin switching occurs in high Gleason grade prostate cancer.** *Prostate.* 2006; **66**(2): 193–9.
PubMed Abstract | Publisher Full Text

71. Bethel CR, Faith D, Li X, *et al.*: **Decreased NKX3.1 protein expression in focal prostatic atrophy, prostatic intraepithelial neoplasia, and adenocarcinoma: association with gleason score and chromosome 8p deletion.** *Cancer Res.* 2006; **66**(22): 10683–90.
PubMed Abstract | Publisher Full Text

72. Ashida S, Nakagawa H, Katagiri T, *et al.*: **Molecular features of the transition from prostatic intraepithelial neoplasia (PIN) to prostate cancer: genome-wide gene-expression profiles of prostate cancers and PINs.** *Cancer Res.* 2004; **64**(17): 5963–5972.
PubMed Abstract | Publisher Full Text

73. Hermeking H, Lengauer C, Polyak K, *et al.*: **14-3-3 sigma is a p53-regulated inhibitor of G2/M progression.** *Mol Cell.* 1997; **1**(1): 3–11.
PubMed Abstract | Publisher Full Text

74. el-Deiry WS, Tokino T, Velculescu VE, *et al.*: **WAF1, a potential mediator of p53 tumor suppression.** *Cell.* 1993; **75**(4): 817–25.
PubMed Abstract

75. Attardi LD, Reczek EE, Cosmas C, *et al.*: **PERP, an apoptosis-associated target of p53, is a novel member of the PMP-22/gas3 family.** *Genes Dev.* 2000; **14**(6): 704–718.
PubMed Abstract | Free Full Text

76. Ongusaha PP, Ouchi T, Kim K, *et al.*: **BRCA1 shifts p53-mediated cellular outcomes towards irreversible growth arrest.** *Oncogene.* 2003; **22**(24): 3749–58.
PubMed Abstract | Publisher Full Text

77. Komarova EA, Diatchenko L, Rokhlin OW, *et al.*: **Stress-induced secretion of growth inhibitors: a novel tumor suppressor function of p53.** *Oncogene.* 1998; **17**(9): 1089–96.
PubMed Abstract | Publisher Full Text

78. Thomas-Tikhonenko A, Viard-Leveugle I, Dews M, *et al.*: **Myc-transformed epithelial cells down-regulate rlusterin, which inhibits their growth *in vitro* and carcinogenesis *in vivo*.** *Cancer Res.* 2004; **64**(9): 3126–3136.
PubMed Abstract | Publisher Full Text

79. Ceballos E, Munoz-Alonso MJ, Berwanger B, *et al.*: **Inhibitory effect of c-Myc on p53-induced apoptosis in leukemia cells. Microarray analysis reveals defective induction of p53 target genes and upregulation of chaperone genes.** *Oncogene.* 2005; **24**(28): 4559–71.
PubMed Abstract | Publisher Full Text

80. Shimono A, Okuda T, Kondoh H: **N-myc-dependent repression of ndr1, a gene identified by direct subtraction of whole mouse embryo cDNAs between wild type and N-myc mutant.** *Mech Dev.* 1999; **83**(1-2): 39–52.
PubMed Abstract | Publisher Full Text

81. Kaplan-Albuquerque N, Bogaert YE, Van Putten V, *et al.*: **Patterns of gene expression differentially regulated by platelet-derived growth factor and hypertrophic stimuli in vascular smooth muscle cells.** *J Biol Chem.* 2005; **280**(20): 19966–19976.
PubMed Abstract | Publisher Full Text

82. Yu J, Liu XW, Kim HR: **Platelet-derived growth factor (PDGF) receptor-alpha-activated c-Jun NH2-terminal kinase-1 is critical for PDGF-induced p21WAF1/CIP1 promoter activity independent of p53.** *J Biol Chem.* 2003; **278**(49): 49582–49588.
PubMed Abstract | Publisher Full Text

83. Butler R, Mitchell SH, Tindall DJ, *et al.*: **Nonapoptotic cell death associated with S-phase arrest of prostate cancer cells via the peroxisome proliferator-activated receptor gamma ligand, 15-deoxy-delta12,14-prostaglandin J2.** *Cell Growth Differ.* 2000; **11**(1): 49–61.
PubMed Abstract

84. Thiery JP, Acloque H, Huang RY, *et al.*: **Epithelial-mesenchymal transitions in development and disease.** *Cell.* 2009; **139**(5): 871–90.
PubMed Abstract | Publisher Full Text

85. Horrevoets AJ, Fontijn RD, van Zonneveld AJ, *et al.*: **Vascular endothelial genes that are responsive to tumor necrosis factor-alpha *in vitro* are expressed in atherosclerotic lesions, including inhibitor of apoptosis protein-1, stannin, and two novel genes.** *Blood.* 1999; **93**(10): 3418–3431.
PubMed Abstract

86. Kalai M, Lamkanfi M, Denecker G, *et al.*: **Regulation of the expression and processing of caspase-12.** *J Cell Biol.* 2003; **162**(3): 457–467.
PubMed Abstract | Publisher Full Text | Free Full Text

87. Mann K, Hainaut P: **Aminothiol WR1065 induces differential gene expression in the presence of wild-type p53.** *Oncogene.* 2005; **24**(24): 3964–75.
PubMed Abstract | Publisher Full Text

88. Manna SK, Mukhopadhyay A, Aggarwal BB: **Human chorionic gonadotropin suppresses activation of nuclear transcription factor-κB and activator protein-1 Induced by tumor necrosis factor.** *J Biol Chem.* 2000; **275**(18): 13307–13314.
PubMed Abstract | Publisher Full Text

89. Xie X, Lu J, Kulbokas EJ, *et al.*: **Systematic discovery of regulatory motifs in human promoters and 3' UTRs by comparison of several mammals.** *Nature.* 2005; **434**(7031): 338–45.
PubMed Abstract | Publisher Full Text | Free Full Text

90. Xiao W, Hodge DR, Wang L: **NF-kappaB activates IL-6 expression through cooperation with c-Jun and IL6-AP1 site, But is independent of its IL6-NFkappaB regulatory site in autocrine human multiple myeloma cells.** *Cancer Biol Ther.* 2004; **3**(10): 1007–17.
PubMed Abstract | Publisher Full Text

91. Garraway LA, Lin D, Signoretti S, *et al.*: **Intermediate basal cells of the prostate: *in vitro* and *in vivo* characterization.** *Prostate.* 2003; **55**(3): 206–18.
PubMed Abstract | Publisher Full Text

92. Schadt EE, Friend SH, Shaywitz DA: **A network view of disease and compound screening.** *Nat Rev Drug Discov.* 2009; **8**(4): 286–95.
PubMed Abstract | Publisher Full Text

93. Nagata Y, Todokoro K: **Requirement of activation of JNK and p38 for environmental stress-induced erythroid differentiation and apoptosis and of inhibition of ERK for apoptosis.** *Blood.* 1999; **94**(3): 853–63.
PubMed Abstract

94. Dong C, Yang DD, Wysk M, *et al.*: **Defective T cell differentiation in the absence of Jnk1.** *Science.* 1998; **282**(5396): 2092–5.
PubMed Abstract | Publisher Full Text

95. Yang CC, Chung A, Ku CY, *et al.*: **NKX3.1 expression and interactions Dataset.** *Figshare.* 2014.
Data Source

Open Peer Review

Current Referee Status: ✓ ✓

Version 1

Referee Report 26 June 2014

doi:10.5256/f1000research.4090.r5066

Philip D. Anderson
Department of Biological Sciences, Salisbury University, Salisbury, MD, USA

This manuscript presents results from multiple experiments identifying and characterizing the interactome of NKX3.1 in immortalized human prostate epithelium (LH) and human prostate cancer cells (LNCaP). The manuscript is well-researched and well-written. This research helps to fulfil an unmet need by the research community, which is to explain the role of NKX3.1 in the prostate epithelium. In that sense, the results are timely. I have only a few comments, questions or points to the authors that need to be addressed.

1. Explain why there are no error bars in Figure 4A?

2. The authors mentioned that they used the 'affy' package in Bioconductor to preprocess their microarray data. Please indicate the affy package version, Bioconductor version, and R version in the methods.

3. The affy package should be cited in the bibliography with this citation: Gautier, L., Cope, L., Bolstad, B. M., and Irizarry, R. A. 2004. affy---analysis of Affymetrix GeneChip data at the probe level. Bioinformatics 20, 3 (Feb. 2004), 307-315.

4. The authors used a heteroscedastic t-test to infer differences in gene expression in their microarray studies. In the methods, please indicate the multiple testing correction that was applied.

5. In *NKX3.1-induced transcriptional program,* final paragraph: There are 331 mRNAs changed >= 3-fold. But in *Pathway analysis*, first paragraph, the 3x dataset is 357 genes. Please explain how these datasets are different?

6. Please indicate the kDa ladder on Figure 3B.

I have read this submission. I believe that I have an appropriate level of expertise to confirm that it is of an acceptable scientific standard.

Competing Interests: No competing interests were disclosed.

Author Response (*Member of the F1000 Faculty* and *F1000Research Advisory Board Member*) 11 Dec 2014

Dieter A Wolf, Tumor Initiation & Maintenance Program / Degenerative Disease Program, Sanford Burnham Prebys Medical Discovery Institute, USA

1. *Explain why there are no error bars in Figure 4A?*

   This figure shows p values from the pathway analysis, which do not have variations.

2. *The authors mentioned that they used the 'affy' package in Bioconductor to preprocess their microarray data. Please indicate the affy package version, Bioconductor version, and R version in the methods.*

   R-version was 2.10.1 and the bioconductor version 2.5 with the appropriate affy package downloaded by the package manager.

3. *The affy package should be cited in the bibliography with this citation: Gautier, L., Cope, L., Bolstad, B. M., and Irizarry, R. A. 2004. affy---analysis of Affymetrix GeneChip data at the probe level. Bioinformatics 20, 3 (Feb. 2004), 307-315.*

   The reference has been included.

4. *The authors used a heteroscedastic t-test to infer differences in gene expression in their microarray studies. In the methods, please indicate the multiple testing correction that was applied.*

   Due to the low number of replicates (2 per time point), no correction was applied. Our rationale is that we initially cast a wider net by basing our gene lists on uncorrected p values. The lists are subsequently validated by the orthogonal method of pathway analysis, where we make the assumption that random changes would not manifest as enriched pathways.

5. *In NKX3.1-induced transcriptional program, final paragraph: There are 331 mRNAs changed >= 3-fold. But in Pathway analysis, first paragraph, the 3x dataset is 357 genes. Please explain how these datasets are different?*

   We apologize for this error, which was corrected. The 3x dataset of 357 genes was used for the analysis.

6. *Please indicate the kDa ladder on Figure 3B.*

   Unfortunately, the original film of this blot which was run in 2007 could not be ascertained. However, Fig 6C shows the expression of GFP and NKX3.1 from the same virus with size markers. The relative sizes of the GFP and NKX3.1 bands are consistent between Fig. 3B and Fig. 6C.

Competing Interests: No competing interests were disclosed.

Referee Report 20 June 2014

doi:10.5256/f1000research.4090.r4848

Kemal S. Korkmaz
Department of Bioengineering, Ege University, İzmir, Turkey

Authors have extensively studied the tumor suppressor function of NKX3.1 using multiple gene expression profiling approaches with validations. Eventually, they have demonstrated the NKX3.1 interactome, which revealed a complex pattern of interactions with DNA damage repair proteins including Ku70, PARP1 and XRCC5 in addition to other transcriptional regulators such as ILF2 and BANF1.

To perform their research, they have used recognized approaches for the analysis of the gene expression patterns upon ectopic expression of NKX3.1 in immortalized human prostate epithelial cells with a basal phenotype, which revealed a rapid and extensive re-programming with 158 mRNAs changing higher than 5-fold and 331 mRNAs changing higher than 3-fold. Since the data obtained and presented here is consistent with the previous reports, especially Bowen *et al.* as well as Erbaykent-Tepedelen *et al.*, suggest that the NKX3.1-induced gene signature is similar to the gene expression pattern found in early human prostate cancers. Therefore, the data give insights about the requirement of the NKX3.1 as a key driver of luminal cell differentiation, its loss allows luminal cells to dedifferentiate into a state with higher proliferative capacity leading to the increased genetic heterogenity, perhaps augmented by concurrent defects in DNA damage repair pathways.

I have read this submission. I believe that I have an appropriate level of expertise to confirm that it is of an acceptable scientific standard.

Competing Interests: No competing interests were disclosed.

Author Response (*Member of the F1000 Faculty* and *F1000Research Advisory Board Member*) 11 Dec 2014

Dieter A Wolf, Tumor Initiation & Maintenance Program / Degenerative Disease Program, Sanford Burnham Prebys Medical Discovery Institute, USA

Since no specific concerns were raised, we thank the reviewer for his efforts!

Competing Interests: No competing interests were disclosed.